

Geochemistry of Mesozoic and Cenozoic sediments in the northern Qaidam basin, northeastern Tibetan Plateau: Implications for provenance and weathering



Xing Jian^a, Ping Guan^{a,*}, Wei Zhang^{a,b}, Fan Feng^a

^a Key Laboratory of Orogenic Belts and Crustal Evolution, Ministry of Education, School of Earth and Space Sciences, Peking University, Beijing 100871, PR China

^b Research Institute of Petroleum Exploration & Development, PetroChina, Beijing 100083, PR China

ARTICLE INFO

Article history:

Received 22 March 2013

Received in revised form 7 October 2013

Accepted 8 October 2013

Available online 17 October 2013

Editor: L. Reisberg

Keywords:

Qaidam basin

Provenance

Chemical weathering

Paleoclimate

CIA

Source composition model

ABSTRACT

Whole-rock geochemical data of the Mesozoic and Cenozoic sediments in the northern Qaidam basin were used to reconstruct the provenance and chemical weathering history. Based on the fairly uniform REE patterns and trace element ratios, both the Mesozoic ($La_{CN}/Yb_{CN} = 10.37 \pm 1.75$; $Eu/Eu^* = 0.68 \pm 0.07$; $Th/Sc = 1.11 \pm 0.38$) and Cenozoic ($La_{CN}/Yb_{CN} = 9.77 \pm 0.62$; $Eu/Eu^* = 0.69 \pm 0.03$; $Th/Sc = 0.97 \pm 0.14$) mudstones were derived from a similar source area with acidic-intermediate rocks as dominant contributors, and two modeled mixtures composed of 60% granite, 35% quartzdiorite and 5% mafic rocks, and 55% granite, 40% quartzdiorite and 5% mafic rocks can be deduced as the potential source compositions for the Mesozoic and Cenozoic sediments, respectively. This conclusion is reinforced by the mudstone major element composition and sandstone petrography. The Early–Middle Jurassic mudstones have relatively high K-corrected CIA (84–93) and PIA (88–99) values, indicating intense chemical weathering conditions; while the Late Jurassic to Cenozoic sediments have variable corrected CIA (51–85) and PIA (50–92) values, implying predominantly mild to moderate weathering conditions. The chemical weathering history suggests that a warm and humid climate prevailed during the Early–Middle Jurassic, whereas a cool and semiarid to arid climate prevailed from the Late Jurassic up to now. This dramatic transition of climate may be attributed to multiple likely factors, including the restructuring of global atmospheric circulation patterns in response to the breakup of Pangea since Late Jurassic, and the orogenic rejuvenation and high elevation of the Qilian Mountains, northeastern Tibetan Plateau. Furthermore, the decreasing chemical weathering intensity over time indicates the increase of aridification and cooling of the climate culminating in the Late Cenozoic.

© 2013 Elsevier B.V. All rights reserved.

1. Introduction

The Qaidam basin is the largest high-altitude terrestrial petroliferous basin in the northeastern Tibetan Plateau (Hanson et al., 2001; Cao et al., 2008) (Fig. 1). An exceptionally thick Mesozoic and Cenozoic sedimentary succession is presented in the basin, with an average thickness up to 8 km (Xia et al., 2001). This succession preserves detailed evidence of the Mesozoic and Cenozoic tectonic and climatic history of the Qaidam basin and related regions. Several significant geologic events such as the collision between Indian and Eurasian plates (Yin and Harrison, 2000; Royden et al., 2008), the formation and uplift of the Tibetan Plateau (Harrison et al., 1992; Tapponnier et al., 2001; Wang et al., 2008; Clark, 2011) and the aridification of Central Asia (Kutzbach et al., 1993; Molnar et al., 1993; Ramstein et al., 1997; An et al., 2001; Dupont-Nivet et al., 2007; Katz et al., 2008; Kent-Corson

et al., 2009; Sun et al., 2010; Zhuang et al., 2011a; Miao et al., 2012) are likely recorded in the succession.

According to the sediment budget, the Mesozoic and Cenozoic multi-stage tectonic uplift events (e.g. Ritts and Biffi, 2001; Zhuang et al., 2011b) and related denudation and unroofing would most likely lead to significant changes of the source rocks for the sediments in the Qaidam basin. Thus provenance interpretations of these sediments can provide useful data for understanding the composition of orogenic belt rocks in the northeastern Tibetan Plateau. Furthermore, the results of provenance analysis also have industrial implications, such as helping to evaluate the relationship between source and sink (e.g. Morton et al., 2004, 2009), discriminating sedimentary systems and depositional areas (e.g. Jian et al., 2013) and thus facilitating oil and gas exploration of the northern Qaidam basin. Although many studies focused on the rocks of the current surrounding mountains of the basin (e.g. Song et al., 2005, 2009; Zhang et al., 2008; Mattinson et al., 2009; Menold et al., 2009; Zhang et al., 2009), detailed provenance studies of the sediments are relatively scarce (e.g. Song B. et al., 2010a; Yang et al., 2013). Sandstone petrography and detrital mineral isotope chronological studies were reported by Ritts and Biffi (2001) and Rieser et al. (2005,

* Corresponding author at: School of Earth and Space Sciences, Peking University, Beijing, 100871, PR China. Tel.: +86 10 62754113.

E-mail addresses: xjian@pku.edu.cn (X. Jian), pguan@pku.edu.cn (P. Guan).

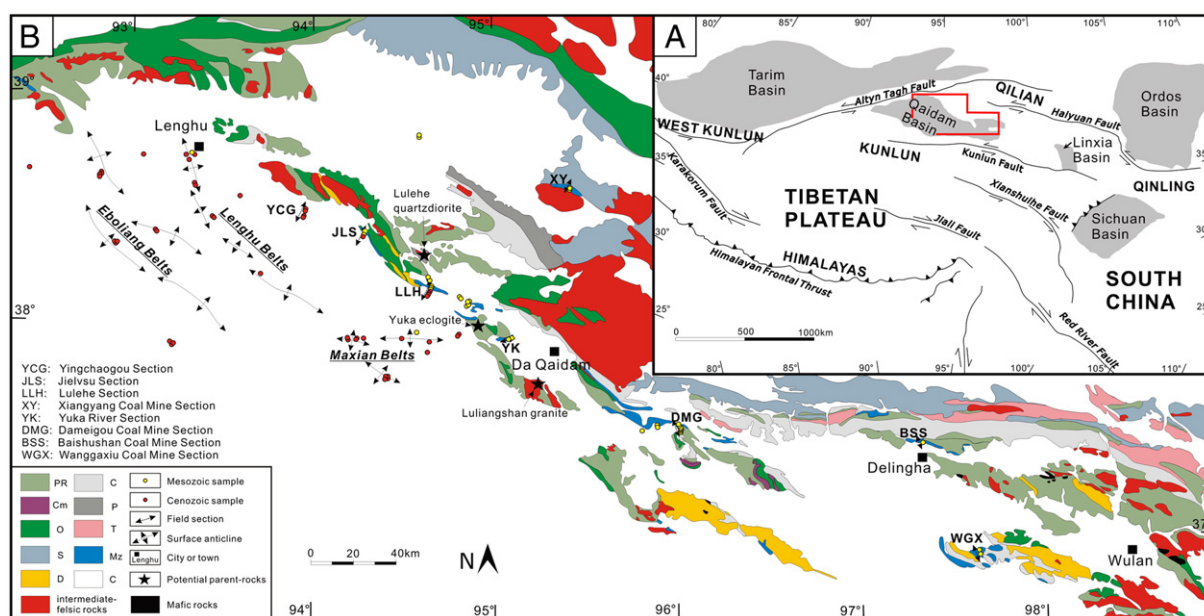


Fig. 1. (A) Tectonic location of the Qaidam basin in the northeastern Tibetan Plateau (modified from [Tapponnier et al., 2001](#)) and (B) geological setting of the northern Qaidam basin and sampling locations.

2006a, 2006b). Their results indicated that the Mesozoic and Cenozoic sediments in the northeastern Qaidam were derived from the Qilian Mountains. [Rieser et al. \(2005\)](#) also reported some geochemical data of mudstones, but they provided little interpretation.

Climatic conditions can control sedimentary environments, and thus influence the sediment generation in the basin. Mudstones, in particular, as the primary hydrocarbon source rocks, are closely connected with the paleoclimatic conditions. Therefore, it is crucial to evaluate the Mesozoic and Cenozoic climatic history of the Qaidam basin. Previous climatic studies of the Qaidam basin mainly concentrated on the stable isotopes of carbonate rocks ([Kent-Corson et al., 2009](#); [Rieser et al., 2009](#); [Zhuang et al., 2011a](#); [Miao et al., 2012](#)) and the pollen composition of sediments ([Wang et al., 1999, 2005, 2007](#); [Miao et al., 2011](#)). These studies mainly focused on the Late Cenozoic aridification, which is generally attributed to the rapid and significant uplift of the Tibetan Plateau ([Kutzbach et al., 1993](#); [Molnar et al., 1993](#); [An et al., 2001](#); [Kent-Corson et al., 2009](#)) and the land–sea redistribution associated with the continental collision of India and Eurasia ([Ramstein et al., 1997](#); [Fluteau et al., 1999](#)). In contrast, climatic study of pre-Late Cenozoic sediments is comparatively scarce. Furthermore, chemical weathering of the Mesozoic and Cenozoic in the northern Qaidam basin has received less attention. In addition, a study of chemical weathering would be a useful complement to the paleoclimatic reconstruction.

Chemical composition of siliciclastic sedimentary rocks is controlled by several factors from source to sink including source rock composition, physical and chemical weathering, erosion, transport, deposition and burial diagenesis ([Johnsson, 1993](#)). Previous studies have demonstrated that the major elements of sedimentary rocks can be used as indicators of source rock character and tectonic setting ([Bhatia, 1983](#); [Roser and Korsch, 1986, 1988](#)). However, their abundances are altered by chemical weathering in the source region ([Nesbitt, 1979](#); [McLennan, 1989](#)), and thus the major-element compositional changes that take place during chemical weathering can be applied to evaluate the weathering history of sedimentary rocks and then to reconstruct the paleoclimatic conditions ([Nesbitt et al., 1980](#); [Nesbitt and Young, 1982, 1984](#); [McLennan et al., 1993](#); [Fedo et al., 1996, 1997](#); [Young, 1999](#)). Furthermore, major-element geochemical data should be used with caution in provenance analysis and weathering reconstruction due to element mobility during diagenesis (e.g. [Nesbitt and Young, 1989](#);

[Fedo et al., 1995](#)). In contrast, several trace elements such as high field strength elements (HFSEs), transition trace elements (TTEs) and rare earth elements (REEs) are considered to be chemically immobile and preserve the signature of source rocks ([Taylor and McLennan, 1985](#); [McLennan, 1989](#); [McLennan et al., 1993](#)). These trace elements are used preferentially for chemical discrimination of sediment source and tectonic setting of sedimentary basins (e.g. [Bhatia and Crook, 1986](#); [Floyd and Leveridge, 1987](#); [McLennan et al., 1993](#)).

In this study, we primarily present major, trace and REE geochemical data and relevant interpretations for the Mesozoic and Cenozoic siliciclastic sediments in the northern Qaidam basin. Petrographic analyses of selected sandstones are also performed. The aims are to: 1) deduce the provenance of these sediments and reconstruct the potential source rock compositions; 2) evaluate the chemical weathering conditions and then reconstruct paleoclimatic evolution of the Qaidam basin.

2. Geological setting

The Qaidam basin lies in the northeastern corner of the Tibetan Plateau ([Fig. 1A](#)) and covers approximately 120,000 km². It sits 2.7–3 km above sea level and contains an exceptionally thick Mesozoic and Cenozoic sedimentary succession of 3–16 km. A peculiar basin-range system is present in the northeastern Tibetan Plateau ([Fig. 1A](#)). The Qaidam basin is bounded by three large mountain ranges which stand up to 5 km above sea level. To the south are Eastern Kunlun Mountains, Qilian Mountains are along the east, and Altun Mountains are to the northwest ([Fig. 1A](#)).

The formation of the current Qaidam basin is regarded as the result of the convergent system in the northeastern Tibetan Plateau ([Tapponnier et al., 2001](#)). Major tectonic events of the Qaidam basin and related areas are shown in [Fig. 2](#). The Mesozoic tectonic settings of the basin are often linked with the evolution of the Meso-Tethys, Neo-Tethys and the Mongol–Okhotsk Ocean and the collisions of related blocks ([Ritts and Biffi, 2001](#); [Kravchinsky et al., 2002](#); [Kapp et al., 2007](#); [Gehrels et al., 2011](#)), while the Cenozoic tectonic evolution of the basin is closely connected with the India–Eurasia collision as well as associated rise, thickening, shortening and lateral extrusion of the Tibetan Plateau ([Harrison et al., 1992](#); [Yue and Liou, 1999](#); [Tapponnier et al., 2001](#); [Yin et al., 2002](#); [Yue et al., 2003](#); [Royden et al., 2008](#)).

Era	Period	Epoch	Time (Ma)	Formation	Abbr.	Sample n=83	Depositional Environment & Lithologic Description	Tectonic Events		
Cenozoic	Quaternary	Holocene					alluvial fan and salt lake environments, the sediments consist of conglomerates, sandstones and evaporites	-(17) Erosion of anticlines internal basin -(16) Folding and basin segmentation		
		Pleistocene	2.8	Qigequan Fm.	Q					
	Neogene	Pliocene		5.3–8	Shizigou Fm.	T ₁	N23	alluvial fan and occasionally fluvio-lacustrine environments, the sediments consist of conglomerates, sandstones and occasionally mudstones and evaporites	-(15) Shrinkage and eastward migration of the lake area -(14) Significant uplift of the surrounding mountains	
				~15	Shang Youshashan Fm.	T ₂	N22			5 mud 2 sand
		Miocene		~22–23	Xia Youshashan Fm.	T ₂	N21	8 mud	fluvial, deltaic and lacustrine environments, the sediments predominantly consist of fine-grained sandstones and mudstones with subordinate carbonate and evaporite layers	-(13) Extensive crustal shortening and thickening of the Tibetan plateau -(12) Qaidam basin pronounced subsidence -(11) Altyn Tagh fault substantial strike-slip
				33.9–35.5	Shang Ganchaigou Fm.	T ₃	N1	5 mud 1 sand		
	Paleogene	Eocene		~45	Xia Ganchaigou Fm.	T ₅	E3	14 mud 5 sand	alluvial fan and plain environments, the sediments consist of red conglomerates with subordinate sandstones and mudstones	-(8) Substantial crustal shortening of the southwestern Qaidam basin North Qaidam and South Qilian -(7) Collision of India and Eurasia
				55.8	Lulehe Fm.	T _R	E1+2	4 mud 1 sand		
		Paleocene		Lack of sediments and erosion phase?						-(6) Closure of Neo-Tethys
	Mesozoic	Cretaceous	Late	65.5	Lack of sediments and erosion phase?					
Early			99.6	Quanyagou Fm.	K1	1 mud 2 sand	alluvial fan and fluvial environments, the sediments consist of red conglomerates and sandstones and occasionally mudstone layers	-(4) Collision of Lhasa Block and Qiangtang Block		
Jurassic		Late	145.5	Hongshuigou Fm.	J3	8 mud 1 sand	fluvial, deltaic and occasionally marginal lacustrine environments, the sediments mainly consist of red sandstone-mudstone suits	-(3) Collision of Siberia block and Mongolia-North China block -(2) Subduction of Meso-Tethys		
		Middle	161	Caishiling Fm. Dameigou Fm.	J2	14 mud 2 sand	fluvial, deltaic, swamp and lacustrine environments, the sediments mainly consist of sandstones, mudstones and coal beds			
		Early	176	Xiaomeigou Fm. Huxishan Fm.	J1	4 mud 3 sand			-(1) Closure of Paleo-Tethys	

Fig. 2. Mesozoic–Cenozoic stratigraphical framework, seismic reflectors (e.g. T₀, T₁), depositional environment and lithological description of the northern Qaidam basin and major tectonic events of this area. mud: mudstone, sand: sandstone, and the front number is the number of analyzed samples in this study. For the details of depositional environment, lithological description and tectonic events and the corresponding references, see Jian (2013).

Consequently, a series of thrust fold belts of NW–SE direction in the basin (Fig. 1B) and reverse faults along Qilian Mountains and Kunlun Mountains were developed, due to the continuous convergence between the Indian and Eurasian plates (Yin and Harrison, 2000; Tapponnier et al., 2001; Yin et al., 2008).

The northern Qaidam basin is closely situated next to Qilian Mountains to the north. It can be divided into two parts: the western area and the eastern area. Several anticlinal belts developed in the western area, including the Lenghu, Maxian and Eboliang belts (Fig. 1B). Hundreds of hydrocarbon exploration wells have been drilled on the belts by PetroChina Qinghai Oilfield Company.

3. Stratigraphy of the northern Qaidam basin

The Mesozoic and Cenozoic strata were deposited mainly in a fluvial–lacustrine depositional environment (Hanson et al., 2001; Ritts and Biffi, 2001; Xia et al., 2001; Zhuang et al., 2011b; Jian, 2013). Based on the basin-wide lithostratigraphic framework and the studies of microfossils, magnetostratigraphy and isotope geochronology (Ye et al., 1993; Sun et al., 2005; Fang et al., 2007; Wang et al., 2007; Lu and Xiong, 2009), the Mesozoic and Cenozoic succession of the Qaidam basin can be divided into the stratigraphic units shown in Fig. 2, together with descriptions of the lithology and depositional environment of each unit. J1 and J2 strata are characterized by gray coal-bearing siliciclastic deposits (Ritts and Biffi, 2001; Wang et al., 2005), J3 and K1 strata mainly consist of red sand-dominant deposits, while the Cenozoic (E1 + 2–Q) strata are composed of mixed evaporite–carbonate–siliciclastic deposits (Feng et al., 2013; Jian, 2013).

4. Sampling and analytical procedures

Eighty-three fresh sedimentary rock samples were collected from eight outcrop sections and thirty drill holes for hydrocarbon exploration

in the northern Qaidam basin (Fig. 1B) for whole-rock geochemical analyses. The details of sample locations and lithology are presented in Tables A1 and A2 (see Appendix A). To facilitate comparison, we refer to the psammitic sediment and pelitic sediment samples as sandstones and mudstones in this study, respectively. Pelitic sediments comprise dominant mudstone and silty mudstone with subordinate coal-bearing mudstone, Fe-bearing mudstone and limy mudstone. In contrast, psammitic sediments include fine-grained to coarser-grained sandstones. The number of mudstone and sandstone samples taken from each stratigraphical unit is presented in Fig. 2. Sandstone samples and related mudstone samples were collected in pairs where possible, in order to aid in evaluating the similarities and differences related to grain size.

Samples for geochemical analysis were first crushed and then powdered to 200 mesh with an agate pulverizer. All sandstones and mudstones were made to thin sections for petrographic observations. The modal analysis of thirteen selected sandstone samples was performed using Gazzi–Dickinson method (Dickinson, 1985). At least 400 points were counted for each sample.

Major elements were determined by X-ray fluorescence spectrometry (XRF, Thermo Arl Advant XP+) at the Key Laboratory of Orogenic Belts and Crustal Evolution, Ministry of Education, Peking University. The sample powders and lithium metaborate flux were mixed in a 1:10 ratio and fused at 1050 °C in a Pt–Au crucible. The resultant melt was cooled and then a glass disk was made for XRF analyses. The values of Loss on ignition (LOI) were obtained by measuring the weight loss after heating the sample at 980 °C. The detailed analytical procedures were given in Liu et al. (2012). The accuracy was estimated to be <2% for all major element oxides (except MnO (4%)) and was monitored using international standards GSR-4 and GSR-5 (Table 1).

The pre-treatment of samples for trace element geochemical analyses was also carried out at Peking University; the procedure is as follows. First, powders were accurately weighed (25 mg) and placed

Table 1

The measured and certified abundances of the major, trace and rare earth elements for the analyzed international standards.

	GSR-5 (shale)		GSR-4 (quartz sandstone)	
	Certified	Measured	Certified	Measured
SiO ₂	59.23	59.33	90.36	90.31
Al ₂ O ₃	18.82	18.54	3.52	3.48
Fe ₂ O ₃ (t)	7.60	7.63	3.22	3.38
CaO	0.60	0.59	0.30	0.29
MgO	2.01	1.98	0.08	0.12
K ₂ O	4.16	4.16	0.65	0.53
Na ₂ O	0.35	0.35	0.06	0.07
MnO	0.02	0.02	0.02	0.02
TiO ₂	0.66	0.66	0.26	0.26
P ₂ O ₅	0.16	0.16	0.22	0.22
LOI	5.95	5.95	1.10	1.10
Li	44	43.0	11.1	10.4
Be	3	2.56	0.97	0.74
Sc	18.5	17.9	4.2	3.68
V	87	82.2	33	32.2
Co	21	25.06	6.4	8.1
Ga	26	23.8	5.3	4.86
Rb	205	203	29	26.8
Sr	90	90.6	58	63.9
Y	26	25.3	21.5	21.1
Zr	96	102	214	229
Nb	14.3	13.6	5.9	5.84
Cs	14	13.8	1.8	1.33
Ba	450	438	143	128
Hf	2.9	3.04	6.6	6.65
Ta	0.9	0.83	0.38	0.39
Pb	8.7	8.25	7.6	7.77
Th	12.8	12.3	7	6.63
U	1.5	1.46	2.1	2.04
La	62	58.3	21	19.6
Ce	109	113	48	45.8
Pr	13.6	12.8	5.4	4.74
Nd	48	49.2	21	19.8
Sm	8.4	8.37	4.7	4.43
Eu	1.7	1.79	1.02	0.96
Gd	6.7	7.21	4.5	4.87
Tb	1.02	0.99	0.79	0.73
Dy	5.1	5.30	4.1	4.18
Ho	0.98	1.01	0.75	0.79
Er	2.7	2.82	2	2.19
Tm	0.43	0.39	0.32	0.30
Yb	2.6	2.55	1.9	1.91
Lu	0.41	0.37	0.3	0.28

The values of major elements and trace elements are in wt.% and ppm, respectively.

in high-pressure-resistant Savillex Teflon beakers, with a 1:1 mixture of HF-HNO₃ and heated for 24 h at 80 °C, and then evaporated. Second, 1.5 ml HNO₃, 1.5 ml HF and 0.5 ml HClO₄ were added respectively after solutions were evaporated to nearly dry, and the beakers with solutions were capped for digestion within a high-temperature oven at 180 °C for at least 48 h until the samples were completely dissolved. Finally, the solutions were diluted with 1% HNO₃ to 50 ml for determination. Trace elements, including REEs, were analyzed using an ELEMENT ICP-MS (Finnigan-MAT Ltd. German) at the Research Institute of Uranium Geology (Beijing). International standards of GSR-4 and GSR-5 (Table 1) were used to monitor analytical quality. The accuracy was estimated to be <10% for all trace elements except Co (19%) and Be (15%).

5. Results

5.1. Sandstone petrography

The Mesozoic and Cenozoic sandstone petrographic observations indicate that most detrital grains are poorly to moderately sorted, angular to subangular (Fig. 3). The point-counting data of sandstone thin sections are shown in Table 2. Overall, the Mesozoic sandstones

contain relatively abundant quartz (e.g. Fig. 3A–B), with a range varying from 61% to 84% (in Q–F–L diagram). Feldspars, dominated by K-feldspar, vary from 6% to 33%. Lithic fragments, composed mainly of metamorphic lithic fragments, are the least abundant components in these sandstones, with abundance ranging from 5% to 16% (Table 2). In comparison, the Cenozoic sandstones are rich in lithic fragments (Fig. A1 in Appendix B), with a range of 19% to 45%, while quartz and feldspars range from 46% to 70% and from 9% to 19%, respectively (Table 2). The lithic fragments are mainly derived from metamorphic sources composed of various metasedimentary rocks, including schist and phyllite (e.g. Fig. 3C–D).

5.2. Major element composition

The major element data are given in Table A3 (see Appendix A). Overall, mudstones show high Al₂O₃ abundances (4.82–29.09 wt.%, av. = 16.27 wt.%) and depletion in SiO₂ (16.62–65.04 wt.%, av. = 52.44 wt.%), whereas sandstones display depletion in Al₂O₃ (4.78–12.87 wt.%, av. = 8.92 wt.%) and enrichment in SiO₂ (48.46–85.85 wt.%, av. = 71.01 wt.%). Therefore, mudstones plot predominantly in the shale field and secondly in the wacke field in the binary diagram between SiO₂/Al₂O₃ and Fe₂O₃/K₂O (Herron, 1988), whereas sandstones can be classed as litharenite, arkose and wacke and subordinate subarkose (Fig. A2 in Appendix B). It is worth noting that J1 and J2 mudstones have higher Al₂O₃ and lower K₂O and Na₂O abundances (Figs. 4B–C, 7), compared to other mudstones.

The elemental compositions of all samples were normalized to the Upper Continental Crust (UCC) (Taylor and McLennan, 1985) composition and are shown in Fig. A3 (see Appendix B). The result indicates that most of the Mesozoic mudstones are highly depleted in Na and Ca, slightly depleted in Si and enriched in Al. Comparatively the Cenozoic mudstones are moderately depleted in Na, slightly depleted in Si and show unobvious enrichment of Al (Fig. A3 in Appendix B). Some samples display distinct enrichment of Ca (e.g. Samples H2-03, YCG-05 and YCG-37b (Table A3)). In contrast, the Mesozoic and Cenozoic sandstones display enrichment of Si and depletion in Al, Na and K (Fig. 4).

5.3. Trace- and rare earth element composition

The trace- and rare earth element data are given in Tables A4 and A5 (see Appendix A). Representative elements and ratios grouped by stratigraphical unit are shown in Fig. 5. The UCC-normalized plots for all analyzed samples are shown in Fig. A3 (Appendix B). Generally, the analyzed mudstones have higher abundances of trace elements than sandstones, with the exception of Sr and Ba (probably due to relatively high abundances of carbonate in sandstones). And mudstones have fairly small ranges of trace element ratios such as Th/Sc and Zr/Sc, whereas sandstones have variable element ratios (Figs. 4F and 5). It is remarkable that all mudstones show similar UCC-normalized trace- and rare earth elemental patterns, while sandstones display variable patterns (Fig. A3 in Appendix B). Furthermore, the Mesozoic mudstones show higher abundances of HFSEs, Th, U and REEs than the Cenozoic mudstones (Figs. 4–5).

REEs were further normalized to chondrites (McDonough and Sun, 1995), and for comparative purposes the REEs of Post-Archean Australian Shale (PAAS) and UCC were also plotted (Fig. 6). Most of the samples show similar patterns to PAAS and UCC, with clear LREE enrichment ($La_N/Yb_N = 6.2–26.2$, av. = 10.1), relatively flat HREE ($Gd_N/Yb_N = 1.2–2.7$, av. = 1.8). All mudstones display significant negative Eu anomalies ($Eu/Eu^* = 0.57–0.82$, av. = 0.69), while sandstones show both negative and positive Eu anomalies ($Eu/Eu^* = 0.62–1.18$, av. = 0.84). Moreover, mudstones show higher abundances of REEs than sandstones (Figs. 4–9), with the ranges from 67.7 to 399.9 ppm (av. = 201.5 ppm), and from 41.4 to 164.3 ppm (av. = 101.6 ppm), respectively.

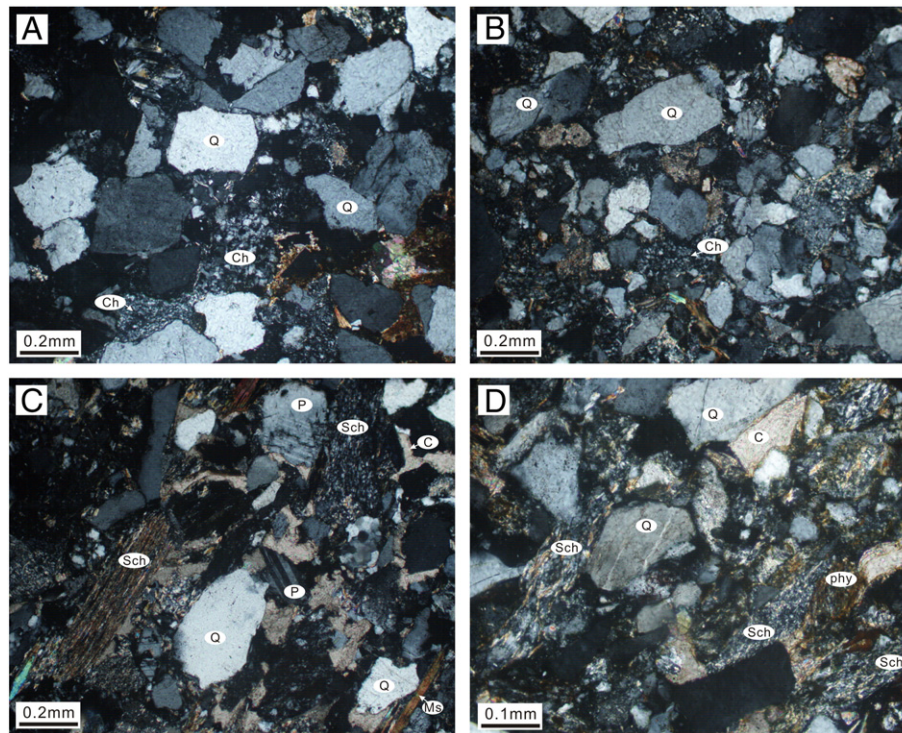


Fig. 3. Representative photomicrographs of sandstone samples. (A–B) J1 sandstones with high quartz abundances from DMG Section (A) and XY Section (B); (C) E3 litharenite from drilling core of Well L87 in Lenghu Belts, characterized by metasedimentary fragments; (D) N22 litharenite from drill core of Well B1 in Maxian Belts. Q: quartz, P: plagioclase, Ch: chert, Sch: schist fragment, Phy: phyllite fragment, Ms: muscovite, C: carbonate.

6. Discussion

The chemical composition of siliciclastic sedimentary rocks results from the combined effects of several factors during sediment production and rock formation. The most commonly documented include, (1) source rock composition and tectonic setting (Bhatia and Crook, 1986; Roser and Korsch, 1988); (2) chemical weathering during the whole sedimentary process and outcrop exposure (Nesbitt and Young, 1982;); (3) grain-size effects due to hydraulic sorting during sediment transport and deposition (McLennan, 1989; McLennan et al., 1993; Cullers, 1994a, b; Singh and Rajamani, 2001); and (4) burial diagenesis and metamorphism (Fedó et al., 1995, 1996). The latter three factors must be evaluated before drawing conclusions on provenance, paleoclimate and tectonic setting of the study area (e.g. Bock et al., 1998; Roddaz et al., 2006; Schoenborn and Fedó, 2011).

6.1. Sedimentary sorting

Hydrodynamical sorting controls the transport of sediments based on grain size, shape and density, which results in a mineralogical and thus chemical differentiation. Studies on modern river bedload and suspended load sediments have indicated that mineral sorting within the water column is a first order control on the chemical composition of sediments (e.g. Garzanti et al., 2010, 2011; Bouchez et al., 2011; Lupker et al., 2011). This leads to a strong heterogeneity of the chemical composition of sediments with different grain sizes. Therefore, it is necessary to account for the effects of sedimentary sorting before chemical weathering and provenance interpretation based on chemical data of sedimentary rocks.

Generally, coarse-grained sediments contain more quartz and feldspar and have thus a low Al/Si ratio, while fine-grained sediments

Table 2
Raw point-counting data of sandstone thin sections.

Sample	Unit	Grain size	Qm	Qp	K	P	Lv	Lm	Ls	Ms	MC	O	Total counts	Q%	F%	L%
DMG-04	J1	c	170	32	48	14	17	32	3	5	138	1	460	64	20	16
DMG-11	J1	m	195	4	60	48	6	13	2	1	152	5	486	61	33	6
XY-06	J1	m	236	4	17	9	0	47	2	3	198	1	517	76	8	16
Y-1	J2	m	323	2	13	10	5	29	5	9	121	7	524	84	6	10
DMG-18	J2	f	184	5	26	12	0	12	1	40	226	8	514	79	16	5
BSS-03	J3	m	165	18	27	13	5	37	0	1	270	4	540	69	15	16
LLH-22	K	f	138	11	35	24	5	24	5	6	169	10	427	62	24	14
X6-02	E3	c	123	1	11	10	2	39	35	0	189	1	411	56	10	34
MB1-01 ^a	E3	m	184	19	16	16	0	46	8	13	40	52	394	70	11	19
B1-02 ^a	E3	c	175	12	20	34	26	43	0	0	93	3	406	60	17	22
L87-08 ^a	N1	m	132	20	18	22	6	84	4	29	70	15	400	53	14	33
NC1-02 ^a	N22	f	138	4	13	30	0	34	11	17	150	3	400	62	19	20
B1-05 ^a	N22	f	104	18	4	21	4	115	0	21	79	7	373	46	9	45

Qm: monocrystalline quartz, Qp: polycrystalline quartz, K: K-feldspar, P: plagioclase, Lv: volcanic lithic fragments, Lm: metamorphic lithic fragments, Ls: sedimentary lithic fragments (carbonate not included), Ms: muscovite and biotite, MC: matrix and cement (including carbonates), O: others (e.g. heavy minerals and opaque minerals), Q = Qm + Qp, F = K + P, L = Lv + Lm + Ls. f: fine sandstone; m: medium sandstone; c: coarse sandstone.

^a The data are from Jian et al. (2013).

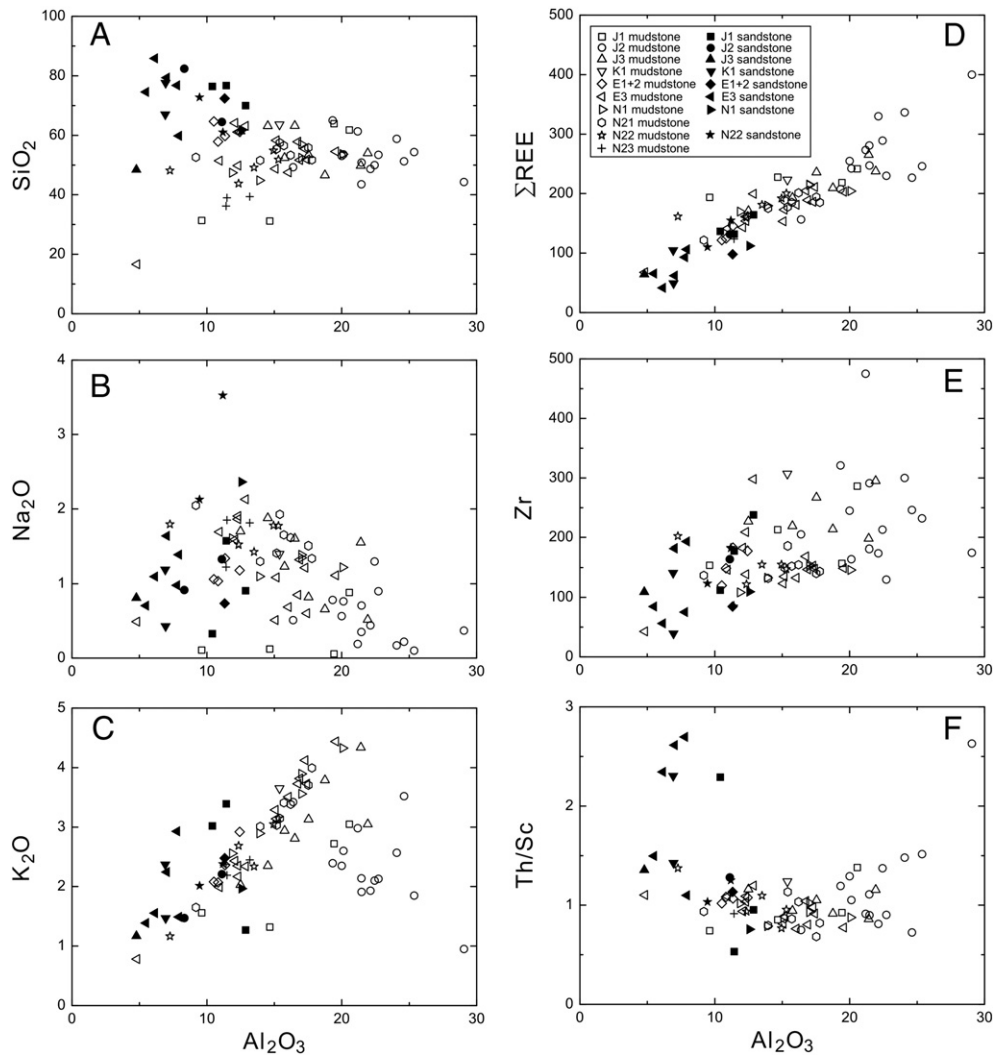


Fig. 4. Binary diagrams of representative major, trace elements and elemental ratio against Al_2O_3 . Note the distinct negative correlation for Al_2O_3 vs. SiO_2 , the significant positive correlation for Al_2O_3 vs. REE and Zr, and no correlation for Al_2O_3 vs. Th/Sc.

tend to be enriched in phyllosilicates and clay minerals that have higher Al/Si ratios (Fig. A2). Although most sandstones and mudstones seemingly have similar REE patterns (Fig. 6), sandstones display comparatively low REE and other trace element abundances (e.g. Th and Zr) and high Eu/Eu^* values (0.62–1.18) (Figs. 5 and A3). The depletion of trace elements in sandstones is likely caused by dilution by quartz, while the distinct Eu anomalies result from the contribution of feldspar (Schnetzler and Philpotts, 1970; Taylor and McLennan, 1985). The high ΣREE in mudstones can be attributed to enrichment of clays, evidenced by their high Al_2O_3 abundances (Fig. 4D). Furthermore, sandstones have wide ranges of elemental ratios (including Eu/Eu^* , Figs. 5 and 7) due to elemental concentration by several specific minerals (for instance, the sandstones with high abundances of plagioclase generally show high Eu/Eu^* values, and the zircon-rich sandstones have high Zr/Sc values) or placer effects with higher and more variable heavy mineral abundances, whereas mudstones have much smaller ranges of trace element ratios (e.g. Th/Sc, La/Th, Figs. 4F, 5 and 7). The similar chondrite-normalized REE patterns (except the Eu anomalies) of sandstones and mudstones (Figs. 5–6) suggest that both sediment groups were likely derived from the same source regions. Consequently, the preceding chemical differentiation between mudstones and the associated sandstones can be attributed to the effect of physical sorting rather than different source rocks.

6.2. Chemical weathering

The influence of chemical weathering, diagenetic K-metasomatism as well as hydrodynamic sorting on the sedimentary rocks, can be visualized in the Al_2O_3 –($\text{CaO}^* + \text{Na}_2\text{O}$)– K_2O (Fig. 7, A–CN–K) ternary diagram (Nesbitt and Young, 1984; Fedo et al., 1995; Nesbitt et al., 1996). Nesbitt and Young (1984) proposed ideal (predicted) weathering trends (Line 2 in Fig. 7) of plutonic and volcanic rocks based on thermodynamic and kinetic considerations. The weathering trend first parallels the A–CN join because plagioclase is more susceptible to chemical weathering than K-feldspar and thus is preferentially destroyed (Grant, 1963; Nesbitt and Young, 1989).

Furthermore, the Chemical Index of Alteration (CIA), devised by Nesbitt and Young (1982), has been widely used to quantify the degree of chemical weathering relative to the source and to reconstruct the paleoweathering conditions of ancient mudstones (e.g. Nesbitt and Young, 1984; Fedo et al., 1995, 1996; Nesbitt et al., 1996; Bock et al., 1998; Roddaz et al., 2006; Schoenborn and Fedo, 2011). $\text{CIA} = [\text{Al}_2\text{O}_3 / (\text{Al}_2\text{O}_3 + \text{CaO}^* + \text{Na}_2\text{O} + \text{K}_2\text{O}) * 100]$ in molecular proportions, where CaO^* represents CaO content in the silicate fraction. In the absence of data on the carbonate content of the sediments, it is difficult to accurately estimate the silicate CaO content. Here we accepted the value of CaO if the mole fraction of $\text{CaO} \leq \text{Na}_2\text{O}$. On the other hand, if $\text{CaO} > \text{Na}_2\text{O}$, then we assumed that the moles of silicate

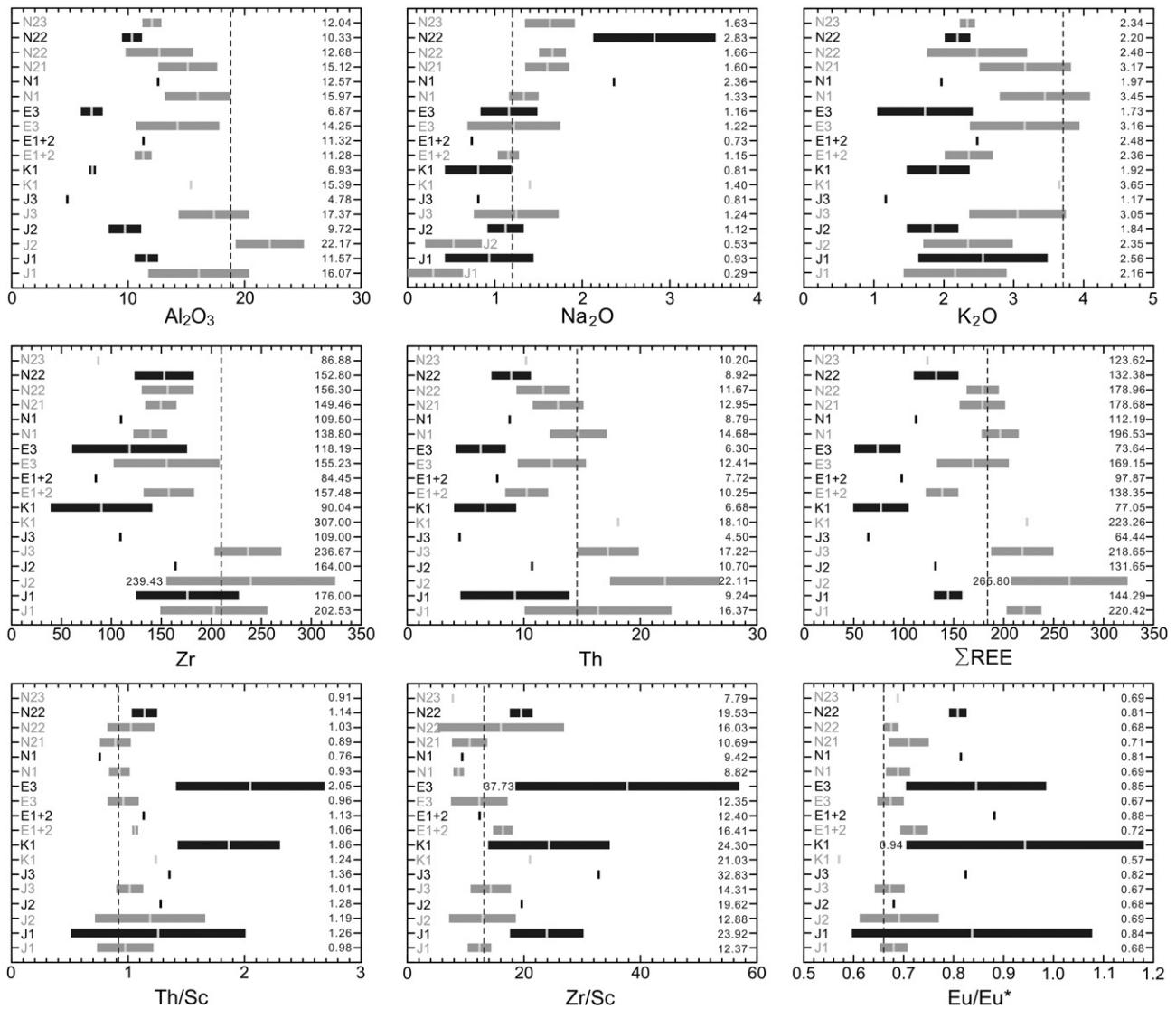


Fig. 5. Stratigraphic variations of representative major, trace and rare earth elements and elemental ratios for mudstones (in gray bar) and sandstones (in black bar). The bar represents standard deviation of the data; the shallow color line inside each bar marks the mean value, which is also given on the right. Note the values of groups with only one sample are shown as short lines. The vertical dashed line, where present, indicates the value of PAAAS (Taylor and McLennan, 1985).

$\text{CaO} = \text{Na}_2\text{O}$ (McLennan, 1993; Bock et al., 1998; Roddaz et al., 2006; Yan et al., 2012).

6.2.1. Effect of sedimentary sorting on weathering intensity evaluation

Hydrodynamic sorting effects the major element compositions of sediments (e.g. Bouchez et al., 2011; Lupker et al., 2011), especially Al and Si contents (Figs. 4, 5 and A2), and thus controls the weathering indices (Garzanti et al., 2011; Lupker et al., 2012). In order to account for the effects of sorting on weathering indices, the sandstone samples and associated mudstone samples collected in pairs (Table A3) are presented in the A–CN–K diagram (Fig. 7A). We assume that the sandstone and the associated mudstone are derived from a same source weathering profile, and hence are subjected to similar weathering conditions. The results show that the mudstones plot closer to the Al apex, while associated sandstones plot near the feldspar join (Fig. 7A), and thus mudstones have higher CIA values than the associated sandstones. This can be explained as follows. Erosion of materials from the source weathering profiles and subsequent hydrodynamic sorting during the transport and deposition process results in separation of mud- and sand-grade materials. The sorting concentrates the aluminous clays in mudstones and the feldspar (and quartz) in sandstones (Nesbitt et al., 1996; Bouchez et al., 2011; Garzanti et al.,

2011; Lupker et al., 2011). Therefore, it is inappropriate to evaluate the chemical weathering intensity with the use of sediments with different grain sizes directly. The CIA values of mudstones are commonly used to evaluate the chemical weathering conditions rather than the CIA values of sandstones in many cases (e.g. Nesbitt et al., 1997; Roddaz et al., 2006; Schoenborn and Fedo, 2011).

The effect of sorting can be easily corrected in modern river sediments (Lupker et al., 2013), whereas it is difficult to correct the weathering indices in ancient sedimentary rocks. The chemical weathering evaluation is based on the mudstone data in this study. Besides, in order to reflect the chemical weathering intensity relative to the source, the CIA values of the sandstones are also inferred by the intersection of Line 4 (Fig. 7A) and the predicted weathering trend (Line 2), since the sediments of different grain sizes from a certain weathering profile, which are subjected to similar chemical weathering conditions, should ideally plot along the vertical line, i.e. Line 4 in Fig. 7A (Nesbitt et al., 1996).

6.2.2. Effect of diagenetic K-metasomatism on weathering intensity evaluation

The effects of sorting do not only produce aluminous muds and quartz- and feldspar-rich sands, but also enhance the K-feldspar:

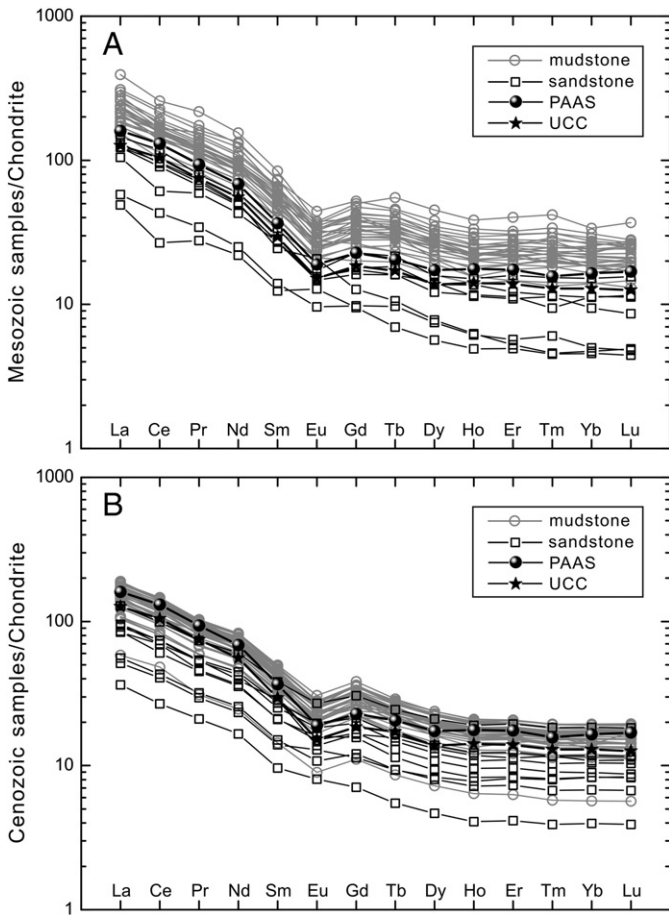


Fig. 6. Chondrite-normalized REE patterns of the (A) Mesozoic and (B) Cenozoic sediments of the northern Qaidam basin. Note the high similarity of LREE enrichment and the negative Eu anomaly for mudstones of each group. The data of chondrite are from McDonough and Sun (1995).

plagioclase ratios in sands relative to the source. According to the trend line of the effects of sorting in the A–CN–K diagram, sands also should have greater Kfs:Pl ratios than the associated muds. However, our investigation of mudstones and sandstone in pairs show that most mudstones deviate from the trend line of the sorting effects (and the predicted weathering trend), plot towards the K_2O apex, and even have more potassium than the associated sandstones (Fig. 7A). Sorting of different size fractions cannot explain the distribution of the data. We advocate that diagenetic K-metasomatism (e.g. conversion of aluminous clay minerals to illite (Fedo et al., 1995)) may strongly change the bulk composition and results in the enrichment of K in most mudstones (especially the Cenozoic mudstones, Fig. 7C). This suggestion is supported by our XRD data, which indicate that these analyzed mudstones have fairly low K-feldspar contents and high illite contents (Jian, 2013). This means that the high K abundances of most mudstones result from the contribution of illite rather than the contribution of K-feldspar. Furthermore, it is remarkable that the degree of K-metasomatism for J3 and the Cenozoic mudstones increased with Al content, whereas most mudstones of J1 and J2 experienced relatively less K-metasomatism. The differentiation may be attributed to the features of formation waters (the J1 and J2 formation waters had low K abundances (data from Qinghai Oilfield Company)).

Hence, the CIA values of mudstones must be corrected due to the effects of K-addition. The procedure of subtracting additional K and CIA correction is illustrated in Fig. 7B and C, and the results are given in Table A3. Additionally, K-corrected CIA values of mudstones are approximately equal to the inferred CIA values of the associated

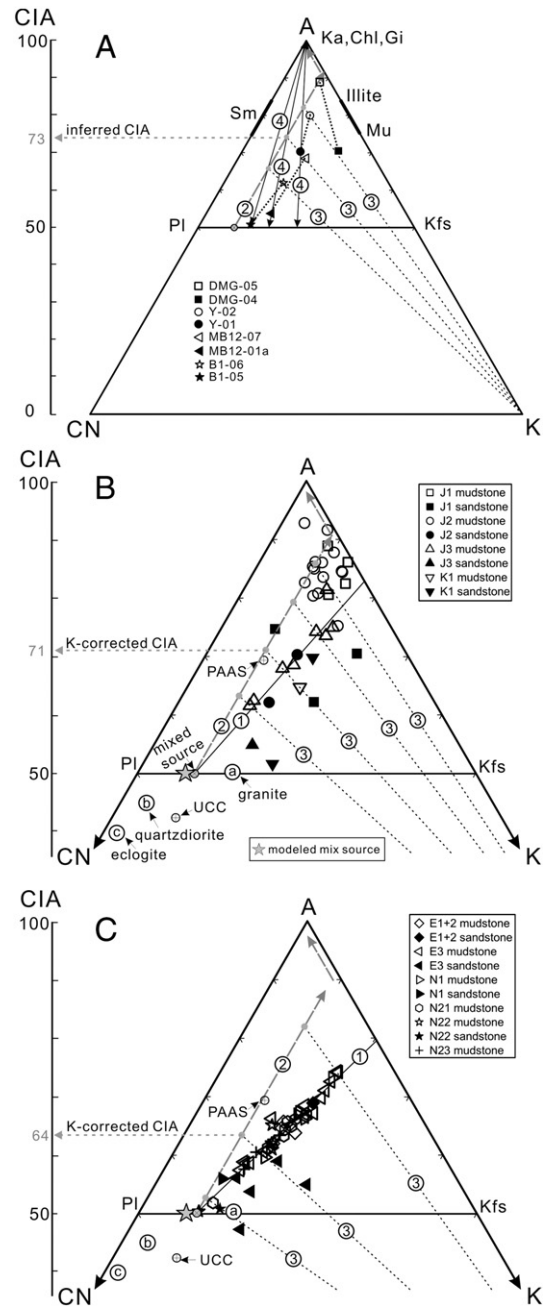


Fig. 7. A–CN–K ternary diagrams for (A) mudstones and the associated sandstones in pairs (connected by dashed lines), all of the (B) Mesozoic and (C) Cenozoic mudstones (open symbols) and sandstones (filled symbols). Solid line (Line 1) is the best-fit straight line through mudstones, and its intersection with feldspar (Pl–Kfs) join indicates the composition of unweathered source rock. Dashed lines with arrows (Line 2) are predicted weathering trends of the unweathered source rock. Line 2 emanates from the unweathered source and extends upwards parallel to the A–CN join until it intercepts the A–K join, then follows the A–K join until the A apex. Correction for K metasomatism is made by projecting data points back onto ideal weathering pathway from K-apex (Line 3) (Fedo et al., 1995, 1997). In this study, for the Mesozoic mudstones, $CIA_{corrected} = [Al_2O_3 / (Al_2O_3 + CaO^* + Na_2O) * (100 - 7.2)]$, for the Cenozoic mudstones, $CIA_{corrected} = [Al_2O_3 / (Al_2O_3 + CaO^* + Na_2O) * (100 - 8.5)]$, where 7.2 and 8.5 represent the molecular percent of K_2O of the unweathered Mesozoic and Cenozoic source rocks, respectively. Note that it is not possible to make a meaningful correction for K-addition when the samples plot above the predicted weathering trend. Vertical solid lines with arrows (Line 4) display the trends of sorting effects, therein, mudstones plot close to the A apex, while sandstones plot near the feldspar join. The inferred CIA values of sandstones are calculated by the intersection of Lines 4 and 2. For the Mesozoic sandstones, $CIA_{inferred} = 100 - 7.2 * [(CaO^* + Na_2O + K_2O) / K_2O]$, for the Cenozoic sandstones, $CIA_{inferred} = 100 - 8.5 * [(CaO^* + Na_2O + K_2O) / K_2O]$. The granite (Point a), quartzdiorite (Point b) and eclogite (Point c) data are from Meng and Zhang (2008), Wu et al. (2009) and Song S. et al. (2010b), respectively. Ka: kaolinite; Chl: chlorite; Gi: Gibbsite; Sm: smectite; Mu: muscovite; Pl: plagioclase; Kfs: K-feldspar.

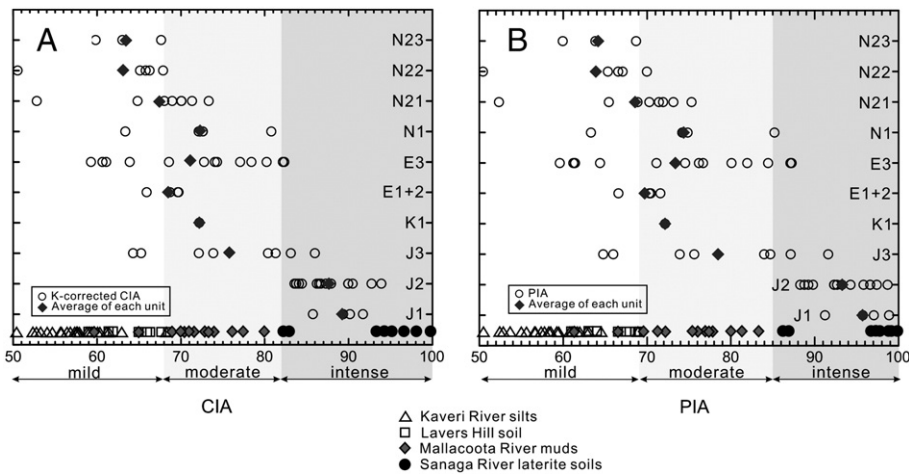


Fig. 8. K-corrected CIA (A) and PIA (B) values of mudstones of each stratigraphical unit. In this study, we classify chemical weathering conditions into three degrees: mild (CIA \approx 50–68, PIA \approx 50–69), moderate (CIA \approx 68–82, PIA \approx 69–86) and intense (CIA \approx 82–100, PIA \approx 86–100) degrees, respectively. Four modern profiles were used in comparison, including Kaveri River silts (mild weathering) of southern India (Singh and Rajamani, 2001), Lavers Hill soil (mild weathering) of southeastern Australia (Duddy, 1980), Mallacoota River muds (moderate weathering) of southeastern Australia (Nesbitt et al., 1996) and Sanaga River laterite soils (intense weathering), East Cameroon (Braun et al., 1997). Note that the main evolution of CIA and PIA values reveals the general decrease in chemical weathering intensity over the sedimentary record.

sandstones (Fig. 7A), which indirectly attests to the influence of K-metasomatism.

Considering the K enrichment problem, Harnois (1988) proposed a new weathering index, i.e. Chemical Index of Weathering (CIW), which eliminates K_2O from the equation ($CIW = [Al_2O_3 / (Al_2O_3 + CaO^* + Na_2O) * 100]$). In the CIW calculation, the possibility that some Al may be included in K-feldspar is not taken into account, and thus this approach is inappropriate when we want to quantify chemical weathering intensity of K-feldspar-rich rocks. Fedo et al. (1995) proposed the Plagioclase Index of Alteration (PIA = $[(Al_2O_3 - K_2O) / (Al_2O_3 + CaO^* + Na_2O - K_2O) * 100]$) as an alternative to the CIW. As plagioclase is abundant in the unweathered source rock (Fig. 7), the PIA is preferred for evaluation of chemical weathering intensity of plagioclase in this study.

6.2.3. CIA and PIA values of mudstones

K-corrected CIA and PIA values of studied mudstones are shown in Table A3 and Fig. 8. The J1 and J2 mudstones have PIA values ranging from 88 to 99. The CIA values of J1 and J2 mudstones range from 82 to 93, with the averages of 88 (4 samples) and 87 (14 samples), respectively (Fig. 8), suggesting intense chemical weathering conditions during the Early–Middle Jurassic. Some of these samples that plot near

the A apex or A–K join (Fig. 7) could have undergone much more intense weathering conditions because it is not possible to make a meaningful correction for subtracting additional K when samples fall into this part of the A–CN–K diagram (Fig. 7). Furthermore, the enrichment of quartz and significant depletion of plagioclase and lithic fragments in most of the sandstones of J1 and J2 (Table 2) also indicate intense weathering. All these results demonstrate that the sediments were mainly derived from the upper zones (e.g. moderately to intensely weathered Zone I and Zone II of Nesbitt et al., 1997) of a developed weathering profile (A weathering profile can be divided into several zones (Nesbitt et al., 1997), therein the upper zones experience intense chemical weathering, whereas the lower zones experience relatively mild chemical weathering). We propose that their source areas experienced mature chemical weathering (characterized by the erosion of upper zones of a weathering profile and sediments composed of stable detritus and aluminous clays). In contrast, the CIA values for mudstones of J3, K1, E1 + 2, E3, N1 and N21 are variable and range from 53 to 85 (Table A3, Fig. 8), with averages of 75, 71 (only one datum for K1), 68, 71, 72, 67 respectively. These mudstones also have variable PIA values ranging from 52 to 92 (Table A3, Fig. 8). Hence, both of these data suggest relatively mild to moderate chemical weathering conditions during Late Jurassic to Early Miocene. Moreover,

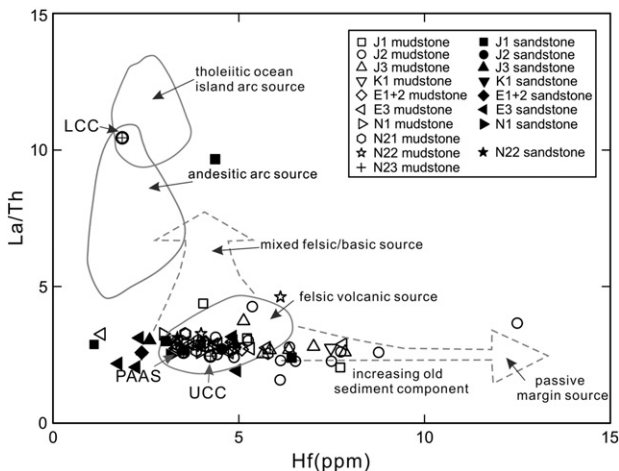


Fig. 9. Plot of La/Th vs. Hf for source rock discrimination (after Floyd and Leveridge, 1987). Note that most samples fall into acidic arc source and some of them have high Hf abundances.

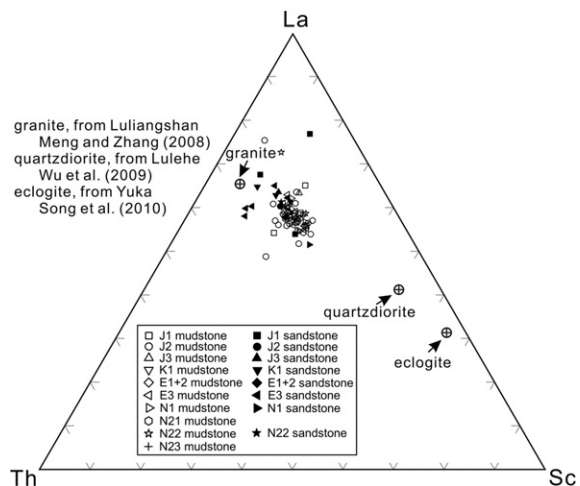


Fig. 10. La–Th–Sc ternary diagram for the sediments. Note that most of the samples are plotted in the area between granite and quartzdiorite.

N22 and N23 mudstones have CIA values ranging from 51 to 68 (Fig. 8), with averages of 63 and 64 respectively. These mudstones also have relatively low PIA values, with a range of 50 to 70, which implies mild weathering conditions since Middle Miocene. Such weathering conditions coincide with the high abundances of lithic fragments (Table 2 and Fig. 3C, D). Thus, both geochemical and petrographic data indicate immature chemical weathering since Late Jurassic, when the sediments were derived from both upper and lower zones of a source weathering profile.

6.3. Provenance of the Mesozoic and Cenozoic sediments

6.3.1. Petrography

Stable lithic fragments such as chert and metaquartzite display high abundances in the Mesozoic J1 and J2 sandstones (Fig. 3A–B), which suggests older sedimentary and metamorphic sources. Unstable lithic

fragments such as schist and phyllite are enriched in the Cenozoic sandstones (Fig. 3C–D), implying that the dominant sources are metasedimentary. In addition, heavy minerals such as zircon, tourmaline, garnet and epidote in these sandstones (Jian, 2013; Jian et al., 2013) also indicate dominant acidic-to-intermediate plutonic and metamorphic sources.

6.3.2. Trace- and rare elements

Some HFSEs (e.g. Th), TTEs (e.g. Co and Sc) and the REEs, have been proven to be useful tools for reconstructing the source composition of sediments (Taylor and McLennan, 1985; McLennan and Taylor, 1991). In the La/Th ratio vs. Hf diagram (Floyd and Leveridge, 1987), the uniformly low La/Th values (varying from 1.58 to 4.62, averaging 2.83, with an exception of 9.67) for all analyzed samples indicate a predominant derivation from a felsic source (Fig. 9). In La–Th–Sc ternary diagram (Fig. 10), all samples plot close to La apex and far

Table 3

Major, trace and rare earth elements of source end members, mixing source and average of mudstones.

Element	End members			Alternative mixture	Mixed source model 1	Mixed source model 2	Mudstone samples			
	Granite	Quartzdiorite	Ecolite	0.65G + 0.35E	0.6G + 0.35GD + 0.05E	0.55G + 0.4GD + 0.05E	Avg. mudstone (Mz)	s.d.	Avg. mudstone (C)	s.d.
<i>Major oxide (wt.%)</i>										
SiO ₂	69.56	53.87	46.85	61.61	62.93	62.15	53.08	8.70	51.99	8.67
TiO ₂	0.45	0.96	2.40	1.13	0.72	0.75	0.84	0.18	0.65	0.13
Al ₂ O ₃	15.21	17.07	15.27	15.23	15.86	15.96	19.59	4.17	13.97	3.19
Fe ₂ O ₃	2.64	7.36	14.32	6.73	4.88	5.11	6.62	5.98	6.02	1.97
MnO	0.04	0.13	0.21	0.10	0.08	0.09	0.14	0.20	0.10	0.05
MgO	0.99	5.79	6.52	2.93	2.95	3.19	1.78	1.01	3.24	1.14
CaO	2.65	7.95	10.06	5.24	4.87	5.14	1.54	2.11	8.44	7.08
Na ₂ O	3.88	3.48	2.62	3.44	3.68	3.66	0.74	0.54	1.39	0.41
K ₂ O	3.18	1.21	0.77	2.34	2.37	2.27	2.58	0.77	2.90	0.83
P ₂ O ₅	0.16	0.18	0.27	0.20	0.17	0.17	0.17	0.13	0.14	0.02
LOI	1.92	3.64	0.70	1.49	2.46	2.55	12.77	8.19	11.00	5.20
Total	100.68	101.62	99.99	100.44	100.97	101.02	99.84	0.12	99.85	0.07
<i>Trace element (ppm)</i>										
Y	18.87	28.80	26.50	21.54	22.72	23.22	35.99	8.49	24.90	4.57
Rb	141.8	40.6	33.8	104.0	101.0	95.9	138.6	36.2	126.0	36.6
Sr	507.8	336.0	319.3	441.8	438.3	429.7	137.9	84.4	249.2	171.7
Ba	814.8	263.5	177.5	591.8	590.0	562.4	535.9	190.8	457.0	94.8
Th	23.05	4.77	1.68	15.57	15.58	14.67	19.86	5.21	12.44	2.76
U	1.82	0.74	0.90	1.50	1.40	1.34	4.94	1.73	3.02	0.94
Zr	222.3	140.5	145.0	195.3	189.8	185.7	235.6	71.5	150.3	38.2
Hf	5.68	3.55	3.54	4.93	4.83	4.72	6.25	1.86	4.20	1.10
Nb	10.97	7.10	18.85	13.73	10.01	9.81	17.73	4.68	12.21	2.30
Ta	0.76	0.45	1.27	0.94	0.68	0.66	1.46	0.43	0.86	0.18
Sc	5.18	26.45	33.26	15.01	14.03	15.09	18.52	4.48	13.38	3.77
Co	5.57	27.25	59.39	24.41	15.85	16.93	18.23	10.35	18.96	5.29
<i>Rare earth element (ppm)</i>										
La	54.13	21.55	15.53	40.62	40.80	39.17	53.97	12.65	35.79	6.68
Ce	103.35	47.15	34.43	79.23	80.23	77.42	99.58	20.25	71.38	13.47
Pr	10.93	5.61	4.62	8.72	8.75	8.48	11.98	2.75	7.87	1.46
Nd	37.40	23.00	20.46	31.47	31.51	30.79	44.30	10.18	30.71	5.65
Sm	6.37	5.08	5.01	5.89	5.85	5.78	8.47	1.76	5.89	1.08
Eu	1.17	1.28	1.80	1.39	1.24	1.24	1.72	0.34	1.33	0.24
Gd	4.82	5.10	5.43	5.03	4.95	4.96	7.21	1.63	5.96	1.13
Tb	0.69	0.84	0.86	0.75	0.75	0.76	1.25	0.29	0.85	0.15
Dy	3.56	5.10	5.36	4.19	4.19	4.26	6.85	1.58	4.78	0.84
Ho	0.66	1.02	1.06	0.80	0.81	0.82	1.32	0.32	0.94	0.17
Er	1.91	3.04	2.95	2.28	2.36	2.42	3.93	0.93	2.75	0.48
Tm	0.27	0.43	0.40	0.31	0.32	0.34	0.61	0.16	0.40	0.07
Yb	1.75	2.73	2.52	2.02	2.13	2.18	3.78	0.83	2.63	0.46
Lu	0.26	0.41	0.37	0.30	0.32	0.32	0.57	0.13	0.39	0.07
∑ REE	227.3	122.3	100.8	183.0	184.2	179.0	245.5	52.0	171.7	31.6
Th/Sc	4.45	0.18	0.05	1.04	1.11	0.97	1.11	0.38	0.96	0.14
La/Th	2.35	4.52	9.22	2.61	2.62	2.67	2.82	0.63	2.92	0.35
Co/Th	0.24	5.71	35.26	1.57	1.02	1.15	0.96	0.48	1.54	0.33
Eu/Eu*	0.65	0.77	1.05	0.78	0.70	0.71	0.68	0.07	0.69	0.03
La _N /Yb _N	22.21	5.66	4.43	14.44	13.74	12.89	10.37	1.75	9.77	0.62
Gd _N /Yb _N	2.28	1.54	1.79	2.06	1.92	1.88	1.59	0.22	1.88	0.10

G: granite, QD: quartzdiorite, E: ecolite, s.d.: standard deviation. The data of granite, quartzdiorite and ecolite are from Meng and Zhang (2008), Wu et al. (2009) and Song S. et al. (2010b), respectively. The proportions of each source end member of the mixed source model were mainly determined by integration of Th/Sc vs. Eu/Eu* (Fig. 11B) and REE patterns (Fig. 12A–B). A total of 66 mudstones were analyzed.

away from Sc apex which also implies a predominant felsic source composition, since Sc is rich in mafic igneous rocks (Taylor and McLennan, 1985; McLennan et al., 1993). Most of them fall into the area between granite (Meng and Zhang, 2008) and quartzdiorite (Wu et al., 2009), indicating the potential mixture of these rocks in the source area. Furthermore, the strong contributions of felsic source rocks are supported by the REE patterns of analyzed samples, which show the characteristics of PAAS-like sediments ($La_N/Yb_N = 7\text{--}15$, $Gd_N/Yb_N = 1.0\text{--}2.0$ and $Eu/Eu^* < 0.85$ (Figs. 6 and A4)).

6.3.3. Detrital zircon ages and detrital garnet chemical compositions

Detrital zircon U–Pb age spectra of sandstones in the northern Qaidam basin are discussed elsewhere (Jian, 2013). The results show that these detrital zircons are composed mainly of Early Paleozoic (clustered at $\sim 400\text{--}480$ Ma) and Late Paleozoic–Early Mesozoic (clustered at $\sim 230\text{--}290$ Ma) grains with subordinate Neoproterozoic (clustered at $\sim 800\text{--}1000$ Ma) and Palaeoproterozoic (clustered at $\sim 1700\text{--}2000$ Ma and $\sim 2300\text{--}2500$ Ma) contributions. Previous paleocurrent measurements indicated general southwest and west directions prevailed in the northern Qaidam basin during the Mesozoic and Cenozoic (Ritts and Biffi, 2001; Zhuang et al., 2011b). And the integrated provenance studies indicated that the source of these sediments could be constrained to be within Qilian Mountains (Ritts and Biffi, 2001; Zhuang et al., 2011b; Jian et al., 2013).

Furthermore, the detrital garnets of sandstones in the northern Qaidam basin are dominated by high Fe + Mn garnets and subordinate high Ca + Mg garnets, indicating that these detrital garnets were predominantly derived from metasedimentary rocks and acidic-to-intermediate igneous rocks but the contribution of mafic rocks cannot be ignored (Jian et al., 2013). However, according to the geochemical discrimination diagrams (e.g. Fig. 9), evidence for a mafic source is almost lost in the whole-rock chemical data of sediments. Thus a mafic end member is also considered in the mixing model discussed below.

6.3.4. Mixed source composition model

Previous studies (Cullers, 1994a, 1994b, 1995) have shown that fine-grained sediments such as shales and siltstones are more likely to have mineralogy and chemical composition similar to their source than coarse-grained sediments and thus they may be better indicators of provenance. Compared to sandstones, mudstones are well homogenized and display fairly uniform elemental ratios (Figs. 5, 9), implying an efficient mixing of source rocks during the sedimentary processes. Hence, in this study, the average composition of mudstones is used to model the mixed source composition.

Major, trace and rare element data of a variety of potential sources were compiled (Table 3) and used to model the relative proportions of end members that contributed sediment to the Mesozoic and Cenozoic strata in the northern Qaidam basin. End members used in the mixing calculation were selected from the representative igneous rocks (or their metamorphic equivalents) in North Qaidam and South Qilian terranes which have published ages close to the detrital zircon age peaks of the sandstones (Jian, 2013). The first end member is a ~ 430 Ma granite exposed in the Luliangshan area (Meng and Zhang, 2008), the second end member is a ~ 271 Ma quartzdiorite exposed in the Lulehe area (Wu et al., 2009), and the third end member is an eclogite (basalt as protolith, magmatic age of ~ 850 Ma) with the metamorphic age of ~ 433 Ma (Song S. et al., 2010b) in the Yuka area. These three end members have distinct trace and rare element characteristics (Table 3, Fig. 11) and thus can provide a wide range of compositions for identifying possible source end member proportions.

Using above-mentioned rock types as the potential source contributors, it is possible to quantitatively model their proportions. The aim of the modeling is to achieve mass balance amongst the REEs, and Th/Sc ratio, both of which are sensitive to bulk source composition (Taylor and McLennan, 1985; McLennan and Taylor, 1991; Fedo et al.,

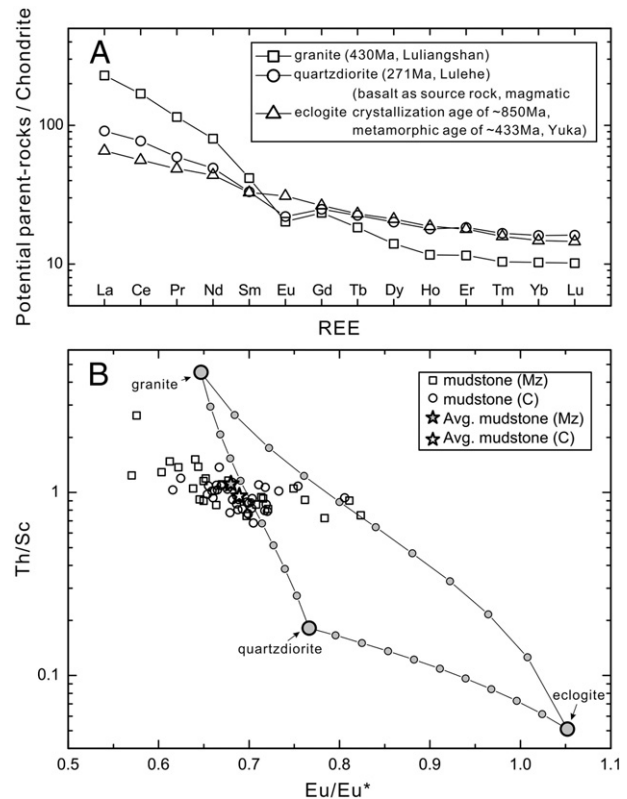


Fig. 11. (A) Chondrite-normalized REE patterns of potential parent-rock end members for the sediments. Three parent-rock end members are recommended. Therein, the data of granite end member are the average of six granite samples from Luliangshan with the zircon SHRIMP U–Pb age of ~ 430 Ma (Meng and Zhang, 2008); the data of quartzdiorite end member are the average of two quartzdiorite samples from Lulehe with the zircon SHRIMP U–Pb age of ~ 271 Ma (Wu et al., 2009); the data of mafic end member are the average of eighteen eclogites from Yuka (Song S. et al., 2010b) with the metamorphic age of ~ 433 Ma. The protolith of these eclogites were regarded as basalts with magmatic crystallization age of ~ 850 Ma (Song S. et al., 2010b). These end members were mixed in order to reproduce an average source area composition. (B) Plot of Th/Sc vs. Eu/Eu^* for mudstones. Mixing curves are divided into 10% increments. A mixture of 60% granite, 35% quartzdiorite and 5% mafic rocks, which balances Th/Sc and Eu/Eu^* values of the average of the Mesozoic mudstones, is proposed as the potential mixed source composition. Likewise, a mixture of 55% granite, 40% quartzdiorite and 5% mafic rocks is proposed as the potential mixed source composition for the Cenozoic mudstones.

1997; Schoenborn and Fedo, 2011). Previous Cenozoic sandstone provenance analysis indicated that the source composition for the sediments of the northern Qaidam basin only has slight variation over time (Jian et al., 2013). Furthermore, the analyzed samples have fairly uniform REE patterns and trace element ratios (Figs. 6, 9). Therefore, in this study, considering the limited number of samples available from each stratigraphic unit, we divide the analyzed mudstone samples into two groups (Fig. 11B), i.e. the Mesozoic mudstones (27 samples) and the Cenozoic mudstones (39 samples), and calculate the average compositions of each mudstone group (Table 3).

A mixture of 60% granite + 35% quartzdiorite + 5% mafic rocks (here, the mafic rock end member is represented by eclogite) is proposed as the ideal modeled source composition for the Mesozoic sediments, because it has a similar chondrite-normalized REE pattern and Th/Sc ratio (and other trace element ratios) to those of the average of the Mesozoic analyzed mudstones (Table 3, Fig. 12A, C). Although the calculated mixed source composition displays slightly lower abundances of REEs than that of the average of mudstones (Fig. 12A, due to enrichment of clays in mudstones), it has a similar negative Eu anomaly and La_N/Yb_N and Gd_N/Yb_N values (Table 3, Fig. 12C). Likewise, a mixture of 55% granite + 40% quartzdiorite + 5% mafic rocks is proposed as the ideal composition of the source for the Cenozoic sediments (Table 3, Fig. 12B, D). Furthermore, the major element compositions of

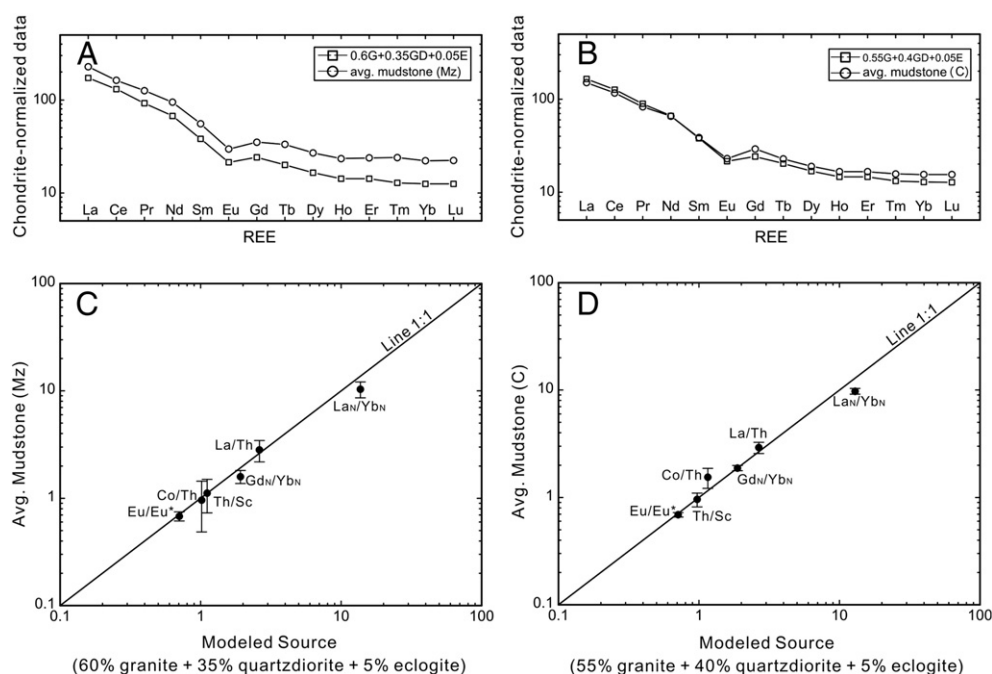


Fig. 12. Comparison between the modeled mixed source and the average mudstone composition. Chondrite-normalized REE patterns (A, B) and trace elemental ratios (C, D) for the Mesozoic (Mz) and Cenozoic (C) sediments. Note that the modeled sources display similar REE patterns and trace element ratios with the average mudstones. High abundances of REEs in mudstones are due to enrichment of clays.

the modeled mixed source (Table 3) demonstrate that the mixture has a plagioclase-K-feldspar ratio of approximately 6:1, very close to that derived from major element data of mudstones in the A–CN–K ternary diagram (Fig. 7). This result reinforces our provenance interpretations.

Although a two-component mixture of 65% granite and 35% mafic rocks (Table 3) also can generate a similar Th/Sc ratio (Th/Sc = 1.03), it has higher La_N/Yb_N (14.4), Gd_N/Yb_N (2.06) and Eu/Eu* (0.78) values, and hence distinctly differs from the averages of the Mesozoic and Cenozoic mudstones. Furthermore, the mafic proportion (35%) of the alternative mixture does not coincide with the low content (maximum approximately 10%) of mafic detrital components (Jian, 2013; Jian et al., 2013). Therefore, the mixture of 60% granite + 35% quartzdiorite + 5% mafic rocks and the mixture of 55% granite + 40% quartzdiorite + 5% mafic rocks provide more appropriate source compositions for the Mesozoic and Cenozoic sediments, respectively.

6.4. Implications for paleoclimatic and tectonic evolution

Here, we reconstruct the Mesozoic and Cenozoic climatic evolutions in the northern Qaidam basin combining chemical weathering intensity, sediment assemblage and depositional environment data, as well as palynological data from the literature. The K-corrected CIA and PIA values of mudstones provide qualitative information about chemical weathering variations over time by plotting as a function of stratigraphic unit (Fig. 8). The details of sediment assemblage and depositional environment for each stratigraphic unit are summarized in Fig. 2.

6.4.1. Early-Middle Jurassic

Overall, the J1 and J2 strata were deposited under warm and humid climatic conditions. The first evidence for warmer and wetter Early-Middle Jurassic climate is provided by coal-bearing sediments (Fig. 2) with abundant higher plant fossils, suggesting open lacustrine and meandering fluvial depositional systems (Ritts and Biffi, 2001). Secondly, this is supported by the evidence for intense chemical weathering (Fig. 8). The labile phases would be easily eliminated (including conversion of feldspars to clay minerals) and the stable phases (e.g. quartz and chert, Fig. 3A–B) would be preserved under

these climatic conditions, which result in high CIA and PIA values for mudstones (Fig. 8). These results are consistent with the dominating hygrophyte and hygro-mesophyte in the palynological assemblages of J1 and J2 strata (Wang et al., 2005). These authors concluded that a general warm temperate-subtropical humid climate prevailed in the Qaidam basin in the early to middle Jurassic (Wang et al., 2005). Furthermore, J1 mudstones have slightly higher CIA and PIA values than J2 mudstone (Fig. 8), which indicates that the Early Jurassic was more humid than the Middle Jurassic, coinciding with the results of trace element geochemical study by Cao et al. (2012).

It is inferred that the humid climatic conditions were likely linked with a strong Early-Middle Jurassic monsoonal circulation, in which Tethyan-derived moisture was transported into the Qaidam basin (Robinson, 1973; Parrish et al., 1982; Hallam, 1984, 1985, 1991). The warm climate could be associated with an enhanced greenhouse effect and a global warming phenomenon due to an increased atmospheric CO₂ content at that time (Hallam, 1985; Chandler et al., 1992; McElwain et al., 1999).

6.4.2. Late Jurassic to Cenozoic

In comparison with the J1–J2 sediments, the J3–N23 strata were deposited under relatively cool and semiarid to arid climatic conditions. The cooler and drier climate since the Late Jurassic is indicated by abundant red beds (Fig. 2), evaporate and calcic paleosol interlayers, dominant fluvial and overbank depositional systems, and the lack of organic-rich rocks, higher plant fossils, and open lacustrine depositional systems (Ritts and Biffi, 2001; Zhuang et al., 2011b). Secondly, a semiarid to arid climate is suggested by the CIA and PIA indices, which are indicative of mild to moderate chemical weathering conditions (Fig. 8). Under these climatic conditions, physical weathering processes such as disaggregation and comminution are likely to predominate over chemical weathering to generate detritus with a mineralogy resembling that of the parent-rocks (e.g. metamorphic lithic fragments, Fig. 3C, D), thus resulting in comparatively low CIA and PIA values for mudstones (Fig. 8). Furthermore, the chemical weathering intensity of the Late Jurassic to Cenozoic displays a decreasing trend over time (Fig. 8), implying the increase of aridification and cooling of the climate during

this stage. The drier climate during the Late Cenozoic is consistent with the palynological data, which illustrated that the Late Cenozoic sediments (mainly from the Middle Miocene to the Quaternary) have higher contents of xerophytic spore-pollen (Wang et al., 1999; Sun and Wang, 2005; Miao et al., 2011).

We infer that the climatic transition starting in the Late Jurassic (from the Early-Middle Jurassic wet and warm climate to the Late Jurassic–Cenozoic arid and cool climate) probably resulted from the breakdown in the monsoonal circulation and the reorganization of global atmospheric circulation patterns in response to the breakup of Pangea (Hallam, 1985; Parrish, 1985, 1992). Locally, we support the viewpoint of Ritts and Biffi (2001), who argued for the orogenic rejuvenation of the Qilian Mountains, thus producing a rain shadow that led to arid conditions. The uplift of the Qilian Mountains is also supported by sedimentary evolution and provenance analysis results (Jian, 2013). Furthermore, the Cenozoic arid climatic conditions of the Qaidam basin were likely controlled by the Paleogene dominant planetary wind system and the Neogene and Quaternary monsoon-dominant system (Wang et al., 1999; Sun and Wang, 2005; Zhang et al., 2007a, 2007b). It has been proven that the East Asian monsoon was markedly intensified and played a leading role in the Asian climate since Late Cenozoic (Shi et al., 1999a, 1999b). The increase of aridification in Central Asia controlled by the Late Cenozoic monsoon-dominant system has been regarded as an integrated result of the uplift of the Tibetan Plateau (e.g. Kutzbach et al., 1993; Molnar et al., 1993; An et al., 2001; Kent-Corson et al., 2009), the retreat of the Paratethys and associated variation of land–sea distribution (Ramstein et al., 1997; Fluteau et al., 1999; Zhang et al., 2007b) and the global cooling (Dupont-Nivet et al., 2007; Katz et al., 2008; Miao et al., 2012). These events and the corresponding paleoclimatic change resulted in relatively mild chemical weathering in the Qaidam basin during the Late Cenozoic and thus lower CIA and PIA values of the mudstones (Fig. 8).

7. Conclusions

This study combines sandstone petrography and major, trace-, and rare earth element geochemistry of the Mesozoic and Cenozoic sediments in the northern Qaidam basin, and yields the following conclusions concerning the source area composition, the chemical weathering conditions, and the paleoclimatic evolution:

- 1) The geochemical differences between sandstones and mudstones can be due to the effects of sedimentary sorting rather than different source rock compositions. According to the fairly uniform chondrite-normalized REE patterns and trace element ratios, these sediments display the characteristics of PAAS-like sediments, and they are likely derived from a source area with dominant felsic bulk compositions.
- 2) The REE pattern and Th/Sc ratio of the Mesozoic and Cenozoic average mudstones are closely reproduced by mixing source rocks exposed in the Qilian Mountains in the following proportions: 60% granite + 35% quartzdiorite + 5% mafic rocks, and 55% granite + 40% quartzdiorite + 5% mafic rocks, respectively, which indicates that acidic-intermediate rocks were the major source contributors for the sediments in the northern Qaidam basin. In addition, this mixture is also compatible with the major element compositions plotted in the A–CN–K diagram.
- 3) The Mesozoic J1 and J2 mudstones have high K-corrected CIA and PIA values and hence experienced relatively intense chemical weathering, which indicates a warm and humid climate. This climate of the Qaidam basin resulted in mature chemical weathering, coinciding with the high contents of stable detritus in the J1 and J2 sandstones. The comparatively low-medium CIA and PIA values of J3–N23 mudstones demonstrate mild to moderate chemical weathering conditions and thus cool and semiarid to arid climate. Additionally, the chemical weathering intensity decreased over

time, suggesting the increase of aridification and cooling of the climate in the northern Qaidam basin.

- 4) The warm and humid Early-Middle Jurassic climate might be related to a strong monsoonal circulation and a global warming phenomenon due to an increased atmospheric CO₂ content. In contrast, the climatic transition since the Late Jurassic may be considered to have resulted from the restructuring of global atmospheric circulation patterns in response to the breakup of Pangea and the orogenic rejuvenation of the Qilian Mountains. Furthermore, the arid and cool Cenozoic climate was probably controlled by the Paleogene planetary wind system pattern and the Neogene and Quaternary monsoon-dominant system. The latter resulted in the increase of aridification and thus relatively mild chemical weathering in the Qaidam basin.

Acknowledgments

This work is supported by the (973) National Basic Research Program of China (Grant No. 2012CB214801), the Major National S&T Program of China (Grant No. 2011ZX05009-002-403, 2011ZX05004-004-005) and the grants from the PetroChina Qinghai Oilfield Company. We thank Ruijuan Liu and Huan Cui for their assistance in sampling. We appreciate Libing Gu, Bin Yang, Fang Ma and Shibiao Deng for their help in laboratory analysis. The Editor Dr. Laurie Reisberg, the reviewer Dr. Maarten Lupker and an anonymous reviewer provided constructive, thoughtful reviews that improved this manuscript. We are grateful to Katie Whitcombe for her significant efforts in improving the English grammar of the manuscript.

Appendix A. Supplementary data

Supplementary data to this article can be found online at <http://dx.doi.org/10.1016/j.chemgeo.2013.10.011>.

References

- An, Z., Kutzbach, J.E., Prell, W.L., Porter, S.C., 2001. Evolution of Asian monsoons and phased uplift of the Himalaya Tibetan plateau since late Miocene times. *Nature* 411, 62–66.
- Bhatia, M.R., 1983. Plate tectonics and geochemical composition of sandstones. *J. Geol.* 91, 611–627.
- Bhatia, M.R., Crook, K.A.W., 1986. Trace element characteristics of graywackes and tectonic setting discrimination of sedimentary basins. *Contrib. Mineral. Petrol.* 92, 181–193.
- Bock, B., McLennan, S.M., Hanson, G.N., 1998. Geochemistry and provenance of the Middle Ordovician Austin Glen Member (Normanskill Formation) and the Taconian Orogeny in New England. *Sedimentology* 45, 635–655.
- Bouchez, J., Gaillardet, J., France-Lanord, C., Maurice, L., Dutra-Maia, P., 2011. Grain size control of river suspended sediment geochemistry: clues from Amazon River depth profiles. *Geochim. Geophys. Geosyst.* 12, Q03008.
- Braun, J.-J., Viers, J., Dupre, B., Polve, M., Ndam, J., Muller, J.-P., 1997. Solid/liquid REE fractionation in the lateritic system of Goyoum, East Cameroon: the implication for the present dynamics of the soil covers of the humid tropical regions. *Geochim. Cosmochim. Acta* 62, 273–299.
- Cao, J., Hu, K., Wang, K., Bian, L.Z., Liu, Y.T., Yang, S.Y., Wang, L.Q., Chen, Y., 2008. Possible origin of 25-norhopanes in Jurassic organic-poor mudstones from the northern Qaidam Basin (NW China). *Org. Geochem.* 39, 1058–1065.
- Cao, J., Wu, M., Chen, Y., Hu, K., Bian, L., Wang, L., Zhang, Y., 2012. Trace and rare earth element geochemistry of Jurassic mudstones in the northern Qaidam Basin, northwest China. *Chem. Erde Geochem.* 72, 245–252.
- Chandler, M.A., Rind, D., Ruedy, R., 1992. Pangaeon climate during the Early Jurassic: GCM simulations and the sedimentary record of palaeoclimate. *Geol. Soc. Am. Bull.* 194, 543–559.
- Clark, M.K., 2011. Early Tibetan Plateau uplift history eludes. *Geology* 39, 991–992.
- Cullers, R.L., 1994a. The chemical signature of source rocks in size fractions of Holocene stream sediment derived from metamorphic rocks in the Wet Mountains region, USA. *Chem. Geol.* 113, 327–343.
- Cullers, R.L., 1994b. The controls on the major and trace element variation of shales, siltstones, and sandstones of Pennsylvanian–Permian age from uplifted continental blocks in Colorado to platform sediment in Kansas, USA. *Geochim. Cosmochim. Acta* 58, 4955–4972.
- Cullers, R.L., 1995. The controls on the major- and trace-element evolution of shales, siltstones and sandstones of Ordovician to Tertiary age in the Wet Mountains region, Colorado, USA. *Chem. Geol.* 123, 107–131.

- Dickinson, W.R., 1985. Interpreting provenance relations from detrital modes of sandstones. In: Zuffa, G.G. (Ed.), *Provenance of Arenites*. Reidel, Dordrecht, pp. 333–336.
- Duddy, I.R., 1980. Redistribution and fractionation of rare-earth and other elements in a weathering profile. *Chem. Geol.* 30, 363–381.
- Dupont-Nivet, G., Krijgsman, W., Langereis, C.G., Abels, H.A., Dai, S., Fang, X., 2007. Tibetan plateau aridification linked to global cooling at the Eocene–Oligocene transition. *Nature* 445, 635–638.
- Fang, X., Zhang, W., Meng, Q., Gao, J., Wang, X., King, J., Song, C., Dai, S., Miao, Y., 2007. High-resolution magnetostratigraphy of the Neogene Huaitoutala section in the eastern Qaidam Basin on the NE Tibetan Plateau, Qinghai Province, China and its implication on tectonic uplift of the NE Tibetan Plateau. *Earth Planet. Sci. Lett.* 258, 293–306.
- Fedo, C.M., Nesbitt, H.W., Young, G.M., 1995. Unraveling the effects of potassium metasomatism in sedimentary rocks and paleosols, with implications for paleoweathering conditions and provenance. *Geology* 23, 921–924.
- Fedo, C.M., Eriksson, K.A., Krogstad, E.J., 1996. Geochemistry of shales from the Archean (3.0 Ga) Buhwa Greenstone Belt, Zimbabwe: implications for provenance and source-area weathering. *Geochim. Cosmochim. Acta* 60, 1751–1763.
- Fedo, C.M., Young, G.M., Nesbitt, H.W., 1997. Paleoclimatic control on the composition of the Paleoproterozoic Serpentine Formation, Huronian Supergroup, Canada: a greenhouse to icehouse transition. *Precambrian Res.* 86, 201–223.
- Feng, J., Cao, J., Hu, K., Peng, X., Chen, Y., Wang, Y., Wang, M., 2013. Dissolution and its impacts on reservoir formation in moderately to deeply buried strata of mixed siliciclastic–carbonate sediments, northwestern Qaidam Basin, northwest China. *Mar. Pet. Geol.* 39, 124–137.
- Floyd, P., Leveridge, B., 1987. Tectonic environment of the Devonian Gramscatho basin, south Cornwall: framework mode and geochemical evidence from turbiditic sandstones. *J. Geol. Soc.* 144, 531–540.
- Fluteau, F., Ramstein, G., Besse, J., 1999. Simulating the evolution of the Asian and African monsoons during the past 30 Myr using an atmospheric general circulation model. *J. Geophys. Res.* 104, 11995–12018.
- Garzanti, E., Ando, S., France-Lanord, C., Vezzoli, G., Censi, P., Galy, V., Najman, Y., 2010. Mineralogical and chemical variability of fluvial sediments: 1. Bedload sand (Ganga–Brahmaputra, Bangladesh). *Earth Planet. Sci. Lett.* 299, 368–381.
- Garzanti, E., Ando, S., France-Lanord, C., Censi, P., Vignola, P., Galy, V., Lupker, M., 2011. Mineralogical and chemical variability of fluvial sediments 2. Suspended-load silt (Ganga–Brahmaputra, Bangladesh). *Earth Planet. Sci. Lett.* 302, 107–120.
- Gehrels, G., Kapp, P., DeCelles, P., Pullen, A., Blakey, R., Weislogel, A., Ding, L., Guynn, J., Martin, A., McQuarrie, N., Yin, A., 2011. Detrital zircon geochronology of pre-Tertiary strata in the Tibetan–Himalayan orogen. *Tectonics* 30, TC5016.
- Grant, W.H., 1963. Weathering of stone mountain granite. In: Ingersoll, E.C. (Ed.), *Clays and Clay Minerals*, 11, pp. 65–73.
- Hallam, A., 1984. Continental humid and arid zones during the Jurassic and Cretaceous. *Palaeogeogr. Palaeoclimatol. Palaeoecol.* 47, 195–223.
- Hallam, A., 1985. A review of Mesozoic climates. *J. Geol. Soc. Lond.* 142, 433–445.
- Hallam, A., 1991. Jurassic climates as inferred from the sedimentary and fossil record. *Philos. Trans. R. Soc. Lond. B* 341, 287–296.
- Hanson, A.D., Ritts, B.D., Zinniker, D., Moldowan, J.M., Biffi, U., 2001. Upper Oligocene lacustrine source rocks and petroleum systems of the northern Qaidam basin, northwest China. *AAPG Bull.* 85, 601–619.
- Harnois, L., 1988. The CIW index: a new chemical index of weathering. *Sediment. Geol.* 55, 319–322.
- Harrison, T.M., Copeland, P., Kidd, W.S.F., Yin, A., 1992. Raising Tibet. *Science* 255, 1663–1670.
- Herron, M.M., 1988. Geochemical classification of terrigenous sands and shales from core or log data. *J. Sediment. Petrol.* 58, 820–829.
- Jian, X., 2013. Controls on Mesozoic and Cenozoic sedimentary evolution of the northern Qaidam basin: tectonic and climatic implications. Unpub. Ph.D. Dissertation, Peking University. (In Chinese with English abstract)
- Jian, X., Guan, P., Zhang, D.-W., Zhang, W., Feng, F., Liu, R.-J., Lin, S.-D., 2013. Provenance of Tertiary sandstone in the northern Qaidam basin, northeastern Tibetan Plateau: integration of framework petrography, heavy mineral analysis and mineral chemistry. *Sediment. Geol.* 290, 109–125.
- Johnsson, M.J., 1993. The system controlling the composition of clastic sediments. In: Johnsson, M.J., Basu, A. (Eds.), *Processes controlling the composition of clastic sediments*. Geological Society of America Special Paper, 284, pp. 1–19.
- Kapp, P., DeCelles, P.G., Gehrels, G.E., Heizler, M., Ding, L., 2007. Geological records of the Lhasa–Qiangtang and Indo-Asian collisions in the Nima area of central Tibet. *Geol. Soc. Am. Bull.* 119, 917–932.
- Katz, M.E., Miller, K.G., Wright, J.D., Wade, B.S., Browning, J.V., Cramer, B.S., Rosenthal, Y., 2008. Stepwise transition from the Eocene greenhouse to the Oligocene icehouse. *Nat. Geosci.* 1, 329–334.
- Kent-Corson, M.L., Ritts, B.D., Zhuang, G., Bovet, P.M., Graham, S.A., Chamberlain, C.P., 2009. Stable isotopic constraints on the tectonic, topographic, and climatic evolution of the northern margin of the Tibetan Plateau. *Earth Planet. Sci. Lett.* 282, 158–166.
- Kravchinsky, V.A., Cogne, J.-P., Harbert, W.P., Kuzmin, M.I., 2002. Evolution of the Mongol–Okhotsk Ocean as constrained by new palaeomagnetic data from the Mongol–Okhotsk suture zone, Siberia. *Geophys. J. Int.* 148, 34–57.
- Kutzbach, J.E., Prell, W.L., Ruddiman, Wm.F., 1993. Sensitivity of Eurasian climate to surface uplift of the Tibetan Plateau. *J. Geol.* 101, 177–190.
- Liu, S., Zhang, J., Li, Q., Zhang, L., Wang, W., Yang, P., 2012. Geochemistry and U–Pb zircon ages of metamorphic volcanic rocks of the Paleoproterozoic Lüliang Complex and constraints on the evolution of the Trans-North China Orogen, North China Craton. *Precambrian Res.* 222–223, 173–190.
- Lu, H., Xiong, S., 2009. Magnetostratigraphy of the Dahonggou section, northern Qaidam Basin and its bearing on Cenozoic tectonic evolution of the Qilian Shan and Altyn Tagh Fault. *Earth Planet. Sci. Lett.* 288, 539–550.
- Lupker, M., France-Lanord, C., Lave', J., Bouchez, J., Galy, V., Me'tivier, F., Gaillardet, J., Lartiges, B., Mugnier, J.-L., 2011. A Rouse-based method to integrate the chemical composition of river sediments: application to the Ganga basin. *J. Geophys. Res.* 116, F04012.
- Lupker, M., France-Lanord, C., Galy, V., Lave', J., Gaillardet, J., Gajurel, A.P., Guilmette, C., Rahman, M., Singh, S.K., Sinha, R., 2012. Predominant floodplain over mountain weathering of Himalayan sediments (Gangabasin). *Geochim. Cosmochim. Acta* 84, 410–432.
- Lupker, M., France-Lanord, C., Galy, V., Lavé, J., Kudrass, H., 2013. Increasing chemical weathering in the Himalayan system since the Last Glacial Maximum. *Earth Planet. Sci. Lett.* 365, 243–252.
- Mattinson, C.G., Wooden, J.L., Zhang, J.X., Bird, D.K., 2009. Paragneiss zircon geochronology and trace element geochemistry, North Qaidam HP/UHP terrane, western China. *J. Asian Earth Sci.* 35, 298–309.
- McDonough, W.F., Sun, S.S., 1995. The composition of the earth. *Chem. Geol.* 120, 223–253.
- McElwain, J.C., Beerling, J., Woodward, F.I., 1999. Fossil plants and global warming at the Triassic–Jurassic boundary. *Science* 285, 1386–1390.
- McLennan, S.M., 1989. Rare earth elements in sedimentary rocks: influence of provenance and sedimentary processes. *Rev. Mineral. Geochem.* 21, 169–200.
- McLennan, S.M., 1993. Weathering and global denudation. *J. Geol.* 101, 295–303.
- McLennan, S.M., Taylor, S.R., 1991. Sedimentary rocks and crustal evolution: tectonic setting and secular trends. *J. Geol.* 99, 1–21.
- McLennan, S.M., Hemming, S., McDaniel, D.K., Hanson, G.N., 1993. Geochemical approaches to sedimentation, provenance and tectonics. *Geol. Soc. Am. Spec. Pap.* 284, 21–40.
- Meng, F.C., Zhang, J.X., 2008. Contemporaneous of Early Palaeozoic granite and high temperature metamorphism, North Qaidam Mountains, western China. *Acta Petrol. Sin.* 24, 1585–1594 (in Chinese with English abstract).
- Menold, C.A., Manning, C.E., Yin, A., Tropper, P., Chen, X.H., Wang, X.F., 2009. Metamorphic evolution, mineral chemistry and thermobarometry of orthogneiss hosting ultrahigh-pressure eclogites in the North Qaidam metamorphic belt, Western China. *J. Asian Earth Sci.* 35, 273–284.
- Miao, Y., Fang, X., Herrmann, M., Wu, F., Zhang, Y., Liu, D., 2011. Miocene pollen record of KC-1 core in the Qaidam Basin, NE Tibetan Plateau and implications for evolution of the East Asian monsoon. *Palaeogeogr. Palaeoclimatol. Palaeoecol.* 299, 30–38.
- Miao, Y., Herrmann, M., Wu, F., Yan, X., Yang, S., 2012. What controlled Mid–Late Miocene long-term aridification in Central Asia? – global cooling or Tibetan Plateau uplift: a review. *Earth Sci. Rev.* 112, 155–172.
- Molnar, P., England, P., Joseph, M., 1993. Mantle dynamics, uplift of the Tibetan plateau and the Indian monsoon. *Rev. Geophys.* 31, 357–396.
- Morton, A.C., Hallsworth, C.R., Chalton, B., 2004. Garnet compositions in Scottish and Norwegian basement terrains: a framework for interpretation of North Sea sandstone provenance. *Mar. Pet. Geol.* 21, 393–410.
- Morton, A., Hallsworth, C., Strogon, D., Whitham, A., Fanning, M., 2009. Evolution of provenance in the NE Atlantic rift: the Early–Middle Jurassic succession in the Heidrun Field, Halten Terrace, offshore Mid-Norway. *Mar. Pet. Geol.* 26, 1100–1117.
- Nesbitt, H.W., 1979. Mobility and fractionation of rare earth elements during weathering of a granodiorite. *Nature* 279, 206–210.
- Nesbitt, H.W., Young, G.M., 1982. Early Proterozoic climates and plate motions inferred from major element chemistry of lutites. *Nature* 299, 715–717.
- Nesbitt, H.W., Young, G.M., 1984. Prediction of some weathering trends of plutonic and volcanic rocks based on thermodynamic and kinetic considerations. *J. Geol.* 48, 1523–1534.
- Nesbitt, H.W., Young, G.M., 1989. Formation and diagenesis of weathering profiles. *J. Geol.* 97, 129–147.
- Nesbitt, H.W., Markovics, G., Price, R.C., 1980. Chemical processes affecting alkalis and alkaline earths during continental weathering. *Geochim. Cosmochim. Acta* 44, 1659–1666.
- Nesbitt, H.W., Young, G.M., McLennan, S.M., Keays, R.R., 1996. Effects of chemical weathering and sorting on the petrogenesis of siliciclastic sediment, with implications for provenance studies. *J. Geol.* 104, 525–542.
- Nesbitt, H.W., Fedo, C.M., Young, G.M., 1997. Quartz and feldspar stability, steady and non-steady-state weathering, and petrogenesis of siliciclastic sands and muds. *J. Geol.* 105, 173–191.
- Parrish, J.T., 1985. Global paleogeography, atmospheric circulation, and rainfall in the Barremian Age (late Early Cretaceous). U.S. Geological Survey Open-File Report, 85-728, p. 13.
- Parrish, J.T., 1992. Jurassic climate and oceanography of the circum-Pacific region. In: Westermann, G.E.G. (Ed.), *The Jurassic of the Circum-Pacific*. IGCP Project 171. Oxford University Press, pp. 365–379.
- Parrish, J.T., Ziegler, A.M., Scotese, C.R., 1982. Rainfall patterns and the distribution of coals and evaporites in the Mesozoic and Cenozoic. *Palaeogeogr. Palaeoclimatol. Palaeoecol.* 40, 67–101.
- Ramstein, G., Fluteau, F., Besse, J., Joussaume, S., 1997. Effect on orogeny, plate motion and land–sea distribution on Eurasian climate change over the past 30 million years. *Nature* 386, 788–795.
- Rieser, A.B., Neubauer, F., Liu, Y., Ge, X., 2005. Sandstone provenance of north-western sectors of the intracontinental Cenozoic Qaidam basin, western China: tectonic vs. climatic control. *Sediment. Geol.* 177, 1–18.
- Rieser, A.B., Liu, Y., Genser, J., Neubauer, F., Handler, R., Friedl, G., Ge, X.-H., 2006a. ⁴⁰Ar/³⁹Ar ages of detrital white mica constrain the Cenozoic development of the intracontinental Qaidam Basin, China. *Geol. Soc. Am. Bull.* 118, 1522–1534.
- Rieser, A.B., Liu, Y., Genser, J., Neubauer, F., Handler, R., Ge, X.-H., 2006b. Uniform Permian ⁴⁰Ar/³⁹Ar detrital mica ages in the eastern Qaidam Basin (NW China): where is the source? *Terra Nova* 18, 79–87.
- Rieser, A.B., Bojar, A., Neubauer, F., Genser, J., Liu, Y., Ge, X.-H., Friedl, G., 2009. Monitoring Cenozoic climate evolution of northeastern Tibet: stable isotope constraints from the western Qaidam Basin, China. *Int. J. Earth Sci.* 98, 1063–1075.

- Ritts, B.D., Biffi, U., 2001. Mesozoic northeast Qaidam basin: response to contractional reactivation of the Qilian Shan, and implications for the extent of Mesozoic intracontinental deformation in central Asia. *Mem. Geol. Soc. Am.* 194, 293–316.
- Robinson, P.L., 1973. Palaeoclimatology and continental drift. In: Tarling, D.H., Runcorn, S.K. (Eds.), *Implications of Continental Drift to the Earth Sciences*, vol. 1. Academic Press, London, pp. 449–476.
- Roddaz, M., Viers, J., Brusset, S., Baby, P., Boucayrand, C., Herail, G., 2006. Controls on weathering and provenance in the Amazonian foreland basin: insights from major and trace element geochemistry of Neogene Amazonian sediments. *Chem. Geol.* 226, 31–65.
- Roser, B.P., Korsch, R.J., 1986. Determination of tectonic setting of sandstone–mudstone suites using SiO₂ content and K₂O/Na₂O ratio. *J. Geol.* 94, 635–650.
- Roser, B.P., Korsch, R.J., 1988. Provenance signatures of sandstone–mudstone suites determined using discriminant function analysis of major–element data. *Chem. Geol.* 67, 119–139.
- Royden, L.H., Burchfiel, B.C., van der Hilst, R.D., 2008. The geological evolution of the Tibetan plateau. *Science* 321, 1054–1058.
- Schnetzler, C.C., Philpotts, J.A., 1970. Partition coefficients of rare-earth elements between igneous matrix material and rock-forming mineral phenocrysts—II. *Geochim. Cosmochim. Acta* 34, 331–340.
- Schoenborn, W.A., Fedo, C.M., 2011. Provenance and paleoweathering reconstruction of the Neoproterozoic Johnnie Formation, southeastern California. *Chem. Geol.* 285, 231–255.
- Shi, Y., Tang, M., Ma, Y., 1999a. Linkage between the second uplifting of the Qinghai–Xizang (Tibetan) Plateau and the initiation of the Asian monsoon system. *Sci. China. Ser. D* 42, 303–312.
- Shi, Y., Li, J., Li, B., Yao, T., Wang, S., Li, S., Cui, Z., Wang, F., Pan, B., Fang, X., Zhang, Q., 1999b. Uplift of the Tibetan Plateau and East Asia environmental change during Late Cenozoic. *Acta Geograph. Sin.* 54, 10–20 (in Chinese with English abstract).
- Singh, P., Rajamani, V., 2001. Geochemistry of the floodplain sediment of the Kaveri River, southern India. *J. Sediment. Res.* 71, 50–60.
- Song, S.G., Zhang, L.F., Niu, Y.L., Su, L., Jian, P., Liu, D.Y., 2005. Geochronology of diamond-bearing zircons from garnet peridotite in the North Qaidam UHPM belt, Northern Tibetan Plateau: a record of complex histories from oceanic lithosphere subduction to continental collision. *Earth Planet. Sci. Lett.* 234, 99–118.
- Song, S., Su, L., Niu, Y., Zhang, G., Zhang, L., 2009. Two types of peridotite in North Qaidam UHPM belt and their tectonic implications for oceanic and continental subduction: a review. *J. Asian Earth Sci.* 35, 285–297.
- Song, B., Zhang, K., Ji, J., Zhang, J., Chen, R., Ye, H., Wang, C., 2010a. Palaeogene sedimentary evolution in the Xitieshan–Changshanliang region, northern Qaidam basin. *Sediment. Geol. Tethyan Geol.* 30, 1–10 (in Chinese with English abstract).
- Song, S., Su, L., Li, X., Zhang, G., Niu, Y., Zhang, L., 2010b. Tracing the 850-Ma continental flood basalts from a piece of subducted continental crust in the North Qaidam UHPM belt, NW China. *Precambrian Res.* 183, 805–816.
- Sun, X., Wang, P., 2005. How old is the Asian monsoon system?—palaeobotanical records from China. *Palaeogeogr. Palaeoclimatol. Palaeoecol.* 222, 181–222.
- Sun, Z., Yang, Z., Pei, J., Ge, X., Wang, X., Yang, T., Li, W., Yuan, S., 2005. Magnetostratigraphy of Paleogene sediments from northern Qaidam Basin, China: implications for tectonic uplift and block rotation in northern Tibetan plateau. *Earth Planet. Sci. Lett.* 237, 635–646.
- Sun, J., Ye, J., Wu, W., Ni, X., Bi, S., Zhang, Z., Liu, W., Meng, J., 2010. Late Oligocene–Miocene mid-latitude aridification and wind patterns in the Asian interior. *Geology* 38, 515–518.
- Tapponnier, P., Xu, Z., Roger, F., Meyer, B., Arnaud, N., Wittlinger, G., Yang, J., 2001. Oblique stepwise rise and growth of the Tibet Plateau. *Science* 294, 1671–1677.
- Taylor, S.R., McLennan, S.M., 1985. *The Continental Crust: Its Composition and Evolution*. Geoscience Texts. Blackwell Scientific Publications 312.
- Wang, J., Wang, Y.J., Liu, Z.C., Li, J.Q., Xi, P., 1999. Cenozoic environmental evolution of the Qaidam Basin and its implications for the uplift of the Tibetan Plateau and the drying of central Asia. *Palaeogeogr. Palaeoclimatol. Palaeoecol.* 152, 37–47.
- Wang, Y., Mosbrugger, V., Zhang, H., 2005. Early to Middle Jurassic vegetation and climatic events in the Qaidam Basin, Northwest China. *Palaeogeogr. Palaeoclimatol. Palaeoecol.* 224, 200–216.
- Wang, X., Qiu, Z., Li, Q., Wang, B., Qiu, Z., Downs, W.R., Xie, G., Xie, J., Deng, T., Takeuchi, G.T., Tseng, Z.J., Chang, M., Liu, J., Wang, Y., Biasatti, D., Sun, Z., Fang, X., Meng, Q., 2007. Vertebrate paleontology, biostratigraphy, geochronology, and paleoenvironment of Qaidam Basin in northern Tibetan Plateau. *Palaeogeogr. Palaeoclimatol. Palaeoecol.* 254, 363–385.
- Wang, C., Zhao, X., Liu, Z., Lippert, P.C., Graham, S.A., Coe, R.S., Yi, H., Zhu, L., Liu, S., Li, Ya, 2008. Constraints on the early uplift history of the Tibetan Plateau. *Proc. Natl. Acad. Sci.* 105, 4987–4992.
- Wu, C., Wooden, J.L., Robinson, P.T., Gao, Y., Wu, S., Chen, Q., Mazdab, F.K., Mattinson, C., 2009. Geochemistry and zircon SHRIMP U–Pb dating of granitoids from the west segment of the North Qaidam. *Sci. China Ser. D Earth Sci.* 52, 1771–1790.
- Xia, W., Zhang, N., Yuan, X., Fan, L., Zhang, B., 2001. Cenozoic Qaidam basin, China: a stronger tectonic inverted, extensional rifted basin. *AAPG Bull.* 85, 715–736.
- Yan, Z., Wang, Z., Yan, Q., Wang, T., Guo, X., 2012. Geochemical constraints on the provenance and depositional setting of the Devonian Liuling Group, East Qinling Mountains, Central China: implications for the tectonic evolution of the Qinling Orogenic Belt. *J. Sediment. Res.* 82, 9–24.
- Yang, Y., Zhang, K., Xu, Y., Song, B., Zhang, J., Luo, M., Ji, J., Chen, F., Chen, R., 2013. Response of the Neogene sedimentary paleocurrent and provenance distribution to uplift of the northeastern Qinghai–Tibetan Plateau. *Acta Geol. Sin.* 87, 797–813 (in Chinese with English abstract).
- Ye, D., Zhong, X., Yao, Y., Yang, F., Zhang, S., Jiang, Z., Wang, Y., 1993. *Tertiary Strata in Chinese Petroleum Provinces (volume I) – the General*. Petroleum Industry Press, Beijing, China (156–159 pp. (in Chinese)).
- Yin, A., Harrison, T.M., 2000. Geologic evolution of the Himalayan–Tibetan orogen. *Annu. Rev. Earth Planet. Sci.* 28, 211–280.
- Yin, A., Rumelhart, P.E., Butler, R.E., Cowgill, E., Harrison, T.M., Foster, D.A., Ingersoll, R.V., Zhang, Q., Zhou, X.-Q., Wang, X.-F., Hanson, A., Raza, A., 2002. Tectonic history of the Altyn Tagh fault system in northern Tibet inferred from Cenozoic sedimentation. *Geol. Soc. Am. Bull.* 114, 1257–1295.
- Yin, A., Dang, Y., Wang, L., Jiang, W., Zhou, S., Chen, X., Gehrels, G.E., McRivette, M.W., 2008. Cenozoic tectonic evolution of Qaidam basin and its surrounding regions (Part 1): the southern Qilian Shan–Nan Shan thrust belt and northern Qaidam basin. *Geol. Soc. Am. Bull.* 120, 813–846.
- Young, G.M., 1999. Some aspects of the geochemistry, provenance and palaeoclimatology of the Torridonian of NW Scotland. *J. Geol. Soc. Lond.* 156, 1097–1111.
- Yue, Y., Liou, J.G., 1999. Two-stage evolution model for the Altyn Tagh fault, China. *Geology* 27, 227–230.
- Yue, Y., Ritts, B.D., Graham, S.A., Wooden, J.L., Gehrels, G.E., Zhang, Z., 2003. Slowing extrusion tectonics: lowered estimate of post–Early Miocene slip rate for the Altyn Tagh fault. *Earth Planet. Sci. Lett.* 217, 111–122.
- Zhang, Z., Wang, H., Guo, Z., Jiang, D., 2007a. Impacts of tectonic changes on the reorganization of the Cenozoic paleoclimatic patterns in China. *Earth Planet. Sci. Lett.* 257, 622–634.
- Zhang, Z., Wang, H., Guo, Z., Jiang, D., 2007b. What triggers the transition of palaeoenvironmental patterns in China, the Tibetan Plateau uplift or the Paratethys Sea retreat? *Palaeogeogr. Palaeoclimatol. Palaeoecol.* 245, 317–331.
- Zhang, G., Song, S., Zhang, L., Niu, Y., 2008. The subducted oceanic crust within continental-type UHP metamorphic belt in the North Qaidam, NW China: evidence from petrology, geochemistry and geochronology. *Lithos* 104, 99–118.
- Zhang, J.-X., Mattinson, C.G., Meng, F.-C., Yang, H.-J., Wan, Y.-S., 2009. U–Pb geochronology of paragneisses and metabasite in the Xitieshan area, north Qaidam Mountains, western China: constraints on the exhumation of HP/UHP metamorphic rocks. *J. Asian Earth Sci.* 35, 245–258.
- Zhuang, G., Hourigan, J.K., Koch, P.L., Ritts, B.D., Kent-Corson, M.L., 2011a. Isotopic constraints on intensified aridity in Central Asia around 12 Ma. *Earth Planet. Sci. Lett.* 312, 152–163.
- Zhuang, G., Hourigan, J.K., Ritts, B.D., Kent-Corson, M.L., 2011b. Cenozoic multiple-phase tectonic evolution of the northern Tibetan Plateau: constraints from sedimentary records from Qaidam basin, Hexi Corridor, and Subei basin, northwest China. *Am. J. Sci.* 311, 116–152.